Microfossil evidence for trophic changes during the Eocene-Oligocene transition in the South Atlantic (ODP Site 1263, Walvis Ridge)

M. Bordiga [1], J. Henderiks [1], F. Tori [2], S. Monechi [2], R. Fenero [3], A. Legarda-Lisarri[1,3], and E. Thomas [4,5]

[1] Department of Earth Sciences, Uppsala University, Villavägen 16, 752 36, Uppsala (Sweden)

[2] Dipartimento di Scienze della Terra, Università di Firenze, Via la Pira 4, I-50121, Florence (Italy)

[3] Departamento de Ciencias de la Tierra and Instituto Universitario de Investigación en Ciencias Ambientales de Aragón, Universidad de Zaragoza, Calle Pedro Cerbuna 12, E−50009, Zaragoza (Spain)

[4] Department of Geology and Geophysics, Yale University, New Haven, CT 06520 (USA)

[5] Department of Earth and Environmental Sciences, Wesleyan University, Middletown, CT 06459 (USA)

Correspondence to: M. Bordiga (manuela.bordiga@geo.uu.se)

Abstract

The biotic response of calcareous nannoplankton to environmental and climatic changes during the Eocene-Oligocene transition was investigated at high resolution at Ocean Drilling Program (ODP) Site 1263 (Walvis Ridge, South East Atlantic Ocean), and compared with a lower resolution benthic foraminiferal record. During this time interval global climate, which had been warm under high levels of atmospheric CO_2 (pCO_2) during the Eocene, transitioned into the cooler climate of the Oligocene, at overall lower pCO_2. At Site 1263, the absolute nannofossil abundance (coccoliths per gram of sediment; N g^{-1}) and the mean coccolith size decreased distinctly after the E-O boundary (EOB; 33.89 Ma), mainly due to a sharp decline in abundance of large-sized *Reticulofenestra* and *Dictyococcites*, occurring within a time-span ~47 kyr. Carbonate dissolution did not vary much across the EOB, thus the decrease in abundance and size of nannofossils may reflect an overall decrease in their export production, which could have led to variations in the food availability for benthic foraminifers.

The benthic foraminiferal assemblage data are consistent with a global decline in abundance of rectilinear species with complex apertures in the latest Eocene (~34.5 Ma), potentially reflecting changes in the food source, thus phytoplankton. This was followed by transient increased abundance of species indicative of seasonal delivery of food to the sea floor (*Epistominella* spp.; ~33.9-33.4 Ma), with a short peak in overall food delivery at the EOB (buliminid taxa; ~33.8 Ma). Increased abundance of *Nuttallides umbonifera* (at ~33.3 Ma) indicates the presence of more corrosive bottom waters, possibly combined arrival of less food at the sea floor after the second step of cooling (Step 2).

The most important changes in the calcareous nannofossil and benthic communities occurred ~120 kyr after the EOB. There was no major change in nannofossil abundance or assemblage composition at Site 1263 after Step 2, although benthic foraminifera indicate more corrosive bottom waters during this time. During the onset of latest Eocene-earliest Oligocene climate change, marine phytoplankton thus showed high sensitivity to fast-changing conditions, as well as to possibly enhanced, pulsed nutrient supply, or to the crossing of a climatic threshold (e.g. pCO_2 decline, high-latitude cooling and changes in ocean circulation).

1 Introduction

The late Eocene-early Oligocene was marked by an important change in global climate and in oceanic environments, reflected in significant biotic turnover. Earth's climate was driven from a warm "greenhouse" with high pCO_2 during the middle Eocene through a transitional period in the late Eocene to a cold "icehouse" at low pCO_2 in the earliest Oligocene (e.g. Zachos et al., 2001; DeConto and Pollard, 2003; Pearson et al., 2009; Pagani et al., 2011; Zhang et al., 2013). During this climate shift, Antarctic ice sheets first reached sea level, sea level dropped, and changes occurred in ocean chemistry and plankton communities, while the calcite compensation depth (CCD) deepened rapidly, at least in the Pacific Ocean (e.g. Zachos et al., 2001; Coxall et al., 2005; Pälike et al., 2006; Coxall and Pearson, 2007; Merico et al 2008). There is ongoing debate whether the overall cooling, starting at high latitudes in the middle Eocene while the low latitudes remained persistently warm until the end of the Eocene (Pearson et al., 2007), was mainly caused by changes in oceanic gateways (opening of Drake Passage and the Tasman gateway) leading to initiation of the Antarctic Circumpolar Current (e.g. Kennett, 1977), or by declining atmospheric CO_2 levels that favored ice sheet growth (e.g. DeConto and Pollard, 2003; Barker and Thomas, 2004; Katz et al., 2008; Goldner et al., 2014) in combination with specific orbital configurations (Coxall et al., 2005), or by some combination of these factors (Sijp et al., 2014). Recently, it has been proposed that the glaciation itself caused further oceanic circulation changes (Goldner et al., 2014; Ladant et al., 2014; Rugenstein et al., 2014).

High-resolution benthic foraminiferal $\delta^{18}O$ records across the Eocene-Oligocene transition (EOT; ~34-33.5 Ma, Pearson et al., 2008) have shown a two-step cooling at several latitudes (e.g. Coxall et al., 2005; Katz et al., 2008; Lear et al, 2008; Coxall and Wilson, 2011; Bohaty et al., 2012). To avoid confusion with previous definitions of these two steps, we follow Pearson et al. (2008) and Bohaty et al. (2012): Step 1 is the first $\delta^{18}O$ increase related to global cooling with a modest ice growth component, and Step 2 is the second increase in $\delta^{18}O$ representing the major ice growth leading to a continental-scale ice sheet over Antarctica (Miller et al., 2009). Foraminifer-based geochemical studies documented the dynamics of the oceanic carbon cycle during the EOT, with an increase in benthic foraminiferal $\delta^{13}C$ which, on kyr-time scales, could relate to an increased ratio in the burial of organic *versus* inorganic carbon (calcite) due to enhanced marine export production and/or increased preservation of organic matter (e.g. Diester-Haass, 1995; Zachos et al., 1996; Coxall and Wilson, 2011). Enhanced export production, however, may not have been global (e.g. Griffith et al., 2010; Moore et al., 2014). The $\delta^{13}C$ shift and oceanic carbon cycle reorganization, linked to increased biological production and deepening of the CCD, have also been related to a rapid drop in pCO_2 (Zachos and Kump, 2005).

There is a strong link between late Eocene-early Oligocene climate change and the response of marine and terrestrial biota. The global cooling, with high extinction rates and ecological reorganization, affected many biological groups, including: calcifying phytoplankton (coccolithophores; e.g. Aubry, 1992; Persico and Villa, 2004; Dunkley Jones et al., 2008; Villa et al., 2008), siliceous plankton (diatoms and radiolarians; e.g. Keller, 1986; Falkowski et al., 2004), planktonic and benthic foraminifers (e.g. Coccioni et al., 1988; Thomas, 1990, 1992; Thomas and Gooday, 1996; Thomas, 2007; Pearson et al., 2008; Hayward et al., 2012), large foraminifers (*Nummulites*; e.g. Adams et al., 1986), ostracods (e.g. Benson, 1975), marine invertebrates (e.g. Dockery, 1986), and mammals (e.g. Meng and McKenna, 1998). Among the marine biota, the planktonic foraminifers experienced a synchronous extinction of five species in the Family Hantkeninidae (e.g. Coccioni et al., 1988; Coxall and Pearson, 2006), the extinction of *Turborotalia cerroazulensis* group and the reduction in size of the *Pseudohastigerina* lineage (Wade and Pearson, 2008 and references therein). Benthic foraminifers experienced a gradual turnover, marked by an overall decline in diversity, largely due to the decline in abundance of cylindrical taxa with a complex aperture (Thomas, 2007; Hayward et al., 2012), and an increase of species which preferentially use fresh phytodetritus delivered to the seafloor in strongly seasonal pulses (e.g. Thomas, 1992; Thomas and Gooday, 1996; Pearson et al., 2008).

Calcareous nannoplankton assemblages underwent significant global restructuring during the EOT, although the group did not suffer extinctions exactly at the Eocene-Oligocene boundary (EOB) in contrast with planktonic foraminifers. Calcareous nannoplankton flourished and diversified during the warm-oligotrophic Eocene, with species diversity at maximum during the early-middle Eocene, decreasing during the cold-eutrophic early Oligocene (Bown et al., 2004). Furthermore, coccolithophores were globally more common and widespread in the Eocene, distinctly declining in (common) occurrence since the early Oligocene (Hannisdal et al., 2012). Species diversity decreased at the expense of specialist taxa, favoring opportunistic species that were more adapted to the new environmental conditions (e.g. Persico and Villa, 2004; Dunkley Jones et al., 2008; Tori, 2008). The decline in diversity of nannoplankton since the middle Eocene coincided with a diversity increase in diatoms, which eventually outcompeted the nannoplankton as the dominant phytoplankton group (e.g. Spencer-Cervato, 1999; Bown et al., 2004; Falkowski et al., 2004).

In addition, the late Eocene to early Oligocene decrease in the average cell size of reticulofenestrids (ancestors of modern-day alkenone producing coccolithophores *Emiliania huxleyi* and *Gephyrocapsa oceanica*) corresponds to a decline in pCO_2 (Henderiks and Pagani, 2008; Pagani et al., 2011). This macroevolutionary trend appears to have been global and primarily caused by the ecological decline of large reticulofenestrid species. Henderiks and Pagani (2008) hypothesized that

large-celled coccolithophores were adapted to high pCO_2 and $CO_{2(aq)}$ conditions (late Eocene), whereas small-sized species are more competitive at lower pCO_2 (early Oligocene). This hypothesis has not yet been tested in detail in the fossil record. Culture experiments, however, provide evidence that elevated levels of CO_2 alleviate carbon-limitation in *E. huxleyi* and *G. oceanica*, and that even these small-celled, bloom-forming coccolithophores operate carbon concentrating mechanisms (CCMs) under today's natural conditions (e.g. Rost et al., 2003; Moolna and Rickaby, 2012). The adaptations in algal carbon acquisition due to lower pCO_2 may have occurred as late as during the late Miocene (about 7-5 million years ago; Bolton and Stoll, 2013), suggesting that Paleogene coccolithophores did not (yet) operate CCMs and that diffusive uptake of CO_2 and growth rates were mainly determined by the volume-to-surface area of the cells.

To date, only few high-resolution studies describe the response of coccolithophores to environmental change along the EOT at high- (Southern Ocean; Persico and Villa, 2004; Villa et al., 2008, 2014) and low latitudes (Tanzania; Dunkley Jones et al., 2008; Fioroni et al., 2015). These studies have highlighted distinct shifts in the composition of the assemblages and decreasing in species diversity at or close to the boundary.

Here, we report on calcareous nannofossil and foraminiferal biotic events between 34.8-32.7 Ma at Ocean Drilling Program (ODP) Site 1263, recovered in the southeast Atlantic Ocean. In particular, we refine the shipboard biostratigraphy published in Zachos et al. (2004), including new data on planktonic foraminifers, and describe the ecological response of calcareous nannoplankton and benthic foraminifers to environmental change during the EOT. The reveal distinct fluctuations in total abundance and taxonomic composition of the calcareous nannofossil assemblages are compared to stable isotope data (Riesselman et al., 2007; Peck et al., 2010), and to benthic foraminiferal assemblage data. For the first time, estimates of the number of nannofossils per gram of dry sediment are calculated for the Eocene-Oligocene time interval to evaluate how paleo-export fluxes and food supply to the benthic community were affected. This is also the first high-resolution (<10,000 yr) record of coccolith size variations (and related changes in mean cell size, cf. Henderiks and Pagani, 2007) across the EOT.

2 Material and methods

2.1 ODP Site 1263

ODP Leg 208 Site 1263 (28°31.97'S and 2°46.77'E, Atlantic Ocean) was drilled at a water depth of 2717 m on the southern flank of Walvis Ridge, an aseismic ridge west of the African coast (Fig. 1).

148 This site provides one of the most continuous sediment sequences of the lower Cenozoic in the
149 Atlantic Ocean, and was at least 1 km above the lysocline prior to the lowering of the CCD during
150 the EOT (Zachos et al., 2004). Foraminifer-bearing nannofossil ooze and nannofossil ooze are the
151 dominant lithologies in the studied interval (Zachos et al., 2004).

152 The Eocene-Oligocene sediments of ODP Site 1263 generally have a high-carbonate content
153 ($CaCO_3$ wt%), ranging from 88 to 96% through 84.2-100.8 mcd (Riesselman et al., 2007). Only a
154 few samples with lower values of $CaCO_3$ (~87%) occur at 99.19 and 99.49 mcd (Riesselman et al.,
155 2007).

156 A total of 190 samples was used for nannofossil analyses across the EOB. Two datasets, A and B,
157 were independently produced at two laboratories and are here combined in a collaborative effort to
158 also demonstrate whether, and how, the primary nannofossil signals are consistently detected from
159 the same sediment cores independent from sample spacing, microscopy slide preparation and
160 operator. Dataset A includes 114 samples from 83.19 to 101.13 meters composite depth (mcd). The
161 sampling resolution is high across the EOB (5-10 cm), and decreases above and below it: 20-90 cm
162 between 83.19-89.6 mcd, and 20-50 cm between 97.44-101.13 mcd. Dataset B includes 76 samples
163 (83.59-105.02 mcd, sampling resolution of 10-50 cm). For analyses on benthic foraminiferal
164 assemblages, 27 samples between 80.89 mcd to 109.79 mcd were used, while for planktonic
165 foraminiferal analysis 16 samples between 93.42 and 107.29 mcd were studied (see Table S1,
166 Supplement).

167

168 **2.2 Microfossil preparation and assemblage counts**

169 **2.2.1 Nannofossils**

170 Sample set A was prepared by weighing 5 mg of dried bulk sediment and diluting with 50 mL of
171 buffered water. Then, 1.5 mL of well-mixed suspension was placed on a cover slip with a high-
172 precision pipette, and the sample was dried on a hotplate at 60°C. This technique (called the "drop
173 technique" by Bordiga et al., 2015; modified after Koch and Young, 2007) avoids selective settling
174 effects because the suspension volume is placed evenly on a cover slip and left to settle and dry
175 under low heat (see Bordiga et al., 2015 for details). Besides assuring slides with an even particle
176 distribution, this preparation technique also allows calculation of the absolute coccolith abundances
177 per gram of dry sediment (N g^{-1}). Repeated sample preparation and counting revealed a coefficient
178 of variation (CV) of 6-10% for absolute abundances (Bordiga et al., 2015), which is comparable to

other techniques (e.g. Bollmann et al., 1999; Geisen et al., 1999). The drop method also provides a good reproducibility for the relative species abundances (Bordiga et al., 2015).

In this study we report on both absolute (N g^{-1}) and relative species abundances (%). Relative abundances are independent from sedimentological effects and estimates of sedimentation rate (e.g. Gibbs et al., 2012), but in contrast to absolute abundances %-values represent a closed-sum, as each percentage value refers to how common or rare a species is relative to other species without knowing whether a species truly increased or decreased in absolute abundance. For these reasons a comparison of both is helpful to evaluate the influence of dilution and sedimentation rate variations, and identify the real fluctuations in abundance of single species. Sample set B was prepared with the standard smear slide technique (Bown and Young, 1998), and the results are given as relative species abundances (%) only.

In both datasets A and B, calcareous nannofossils were examined under polarized light microscopy (LM) at 1000X magnification. At least 300 specimens were counted in each slide. Additional observations were performed on the slide to detect the occurrence of rare species, especially biostratigraphical markers. All specimens were identified at species or genus level, depending on the coccolith preservation. We used *Cyclicargolithus* spp. to group the specimens with dissolved central area that can be associated to the genus *Cyclicargolithus* but not directly to the species *Cyclicargolithus floridanus* (Fig. S1, Supplement). Taxonomy of the calcareous nannofossils follows the references contained in the web-site http://ina.tmsoc.org/Nannotax3 (edited by Young et al., 2014). Additional taxonomical remarks are given in the Supplement. For dataset A, the number of fields of view (FOV) observed were also noted in order to calculate absolute abundances. An average of 26 FOVs (=0.31 mm^2) was observed along the sequence, from a minimum of 18 FOVs (=0.21 mm^2) to a maximum of 44 FOVs (=0.52 mm^2). Both datasets were used to provide biostratigraphical information: dataset A with a more detailed resolution across the EOB, and dataset B covering a longer interval below the EOB.

2.2.2 Foraminifers

The samples were oven-dried at 60°C, then washed over a 63 μm sieve. The complete > 63 μm size fraction was used for the study of benthic foraminifers. Taxa were generally determined at species level (Fenero et al., 2010) and relative abundances were calculated. The benthic foraminiferal studies were on the number of foraminifers in the full sample. All specimens were picked from material spread out in a picking tray, and mounted on microslides for identification, then deposited

211 in the Department of Earth Sciences, University of Zaragoza (Spain). The planktonic foraminiferal
212 assemblages were observed in the >63 μm fraction to determine the presence of biostratigraphical
213 markers, such as the *Turborotalia cerroazulensis* group and species of the Family Hantkeninidae.
214 The presence or absence of tubulospines was noted (Table S1, Supplement). The reduction in size
215 of the *Pseudohastigerina* lineage was observed by counting the number of *Pseudohastigerina micra*
216 and *Pseudohastigerina naguewichiensis* in a total of 300 planktonic foraminifers in the 150-250 μm
217 and 125-150 μm fractions (cf. Wade and Pearson, 2008; Table S1, Supplement).

218

219 **2.3 Biotic proxies**

220 **2.3.1 Nannofossil dissolution index and cell size estimates**

221 Sample set A was used to characterize nannofossil dissolution across the investigated interval. A
222 coccolith dissolution index was calculated using the ratio between entire coccoliths and fragments
223 (cf. Beaufort et al. 2007; Blaj et al., 2009; Pea, 2010). This index is indicative of the
224 preservation/dissolution state of the nannofossil assemblages: higher values correspond to better
225 preservation. Entire coccoliths and all fragments were counted until at least 300 entire coccoliths
226 had been counted. Only pieces bigger than 3 μm were considered as fragments.

227 Mean coccolith and cell size estimates (volume-to-surface area ratio, V:SA; cf. Henderiks and
228 Pagani, 2007; Henderiks, 2008) were calculated based on the relative abundance and size range (3-7
229 μm, 7-11 μm and 11-16 μm for *Coccolithus*; 3-5 μm, 5-7 μm and 7-9 μm for all the other species)
230 of placolith-bearing taxa (*Coccolithus*, *Cyclicargolithus*, *Dictyococcites* and *Reticulofenestra*).

231

232 **2.3.2 Calcareous nannofossil paleoecology**

233 The distribution of coccolithophores in sea surface waters is controlled by the availability of light,
234 temperature, salinity and nutrient availability (e.g. Winter et al., 1994). Studies of modern and past
235 paleogeographic distributions of coccolithophores, allow determination of (paleo)environmental
236 tolerances of various taxa (see Table 3 in Villa et al., 2008). However, some paleoecological
237 interpretations remain unresolved, or contradictory between different regions (see Table 3 in Villa
238 et al., 2008). Therefore, we aimed to circumvent problems in interpretation by not tagging certain
239 (groups of) species *a priori*, but instead investigating the behaviour within assemblages (see Section
240 2.4) and then compare these with independent proxies (i.e. geochemical and benthic foraminiferal
241 assemblage data).

2.3.3 The $\delta^{13}C$ gradient in foraminiferal tests

The difference between planktonic and benthic foraminiferal carbon isotope values ($\Delta\delta^{13}C_{p-b}$) was proposed as a semi-quantitative proxy of paleoproductivity (Sarnthein and Winn 1990). It provides information about the surface to deep-water gradient in $\delta^{13}C$ in Dissolved Inorganic Carbon (DIC), reflecting a combination of surface paleoproductivity and ocean circulation and stratification (e.g. Zhang et al., 2007; Bordiga et al., 2013). We calculated the $\Delta\delta^{13}C_{p-b}$ using data in Riesselman et al. (2007) and Peck et al. (2010).

2.3.4 Benthic foraminifers as paleoenvironmental proxies

We determined the relative abundances of benthic foraminiferal taxa, and the diversity of the assemblages, expressed as the Fisher's alpha index (Hayek and Buzas, 2010). Changes in the relative abundances and diversity were used to infer changes in carbonate saturation state, oxygenation and food supply (e.g. Bremer and Lohmann, 1982; Jorissen et al., 1995, 2007; Gooday, 2003; Thomas, 2007; Gooday and Jorissen, 2012).

The relative abundance of infaunal benthic foraminiferal taxa has been linked to a combination of oxygenation and food supply ('TROX model; Jorissen et al., 1995, 2007; Gooday, 2003), with high relative abundances reflecting a high food supply, extreme low oxygenation levels, or some combination of both. In addition, calcifying infaunal dwellers may gain an advantage over epifaunal dwellers during deep-water acidification (Foster et al., 2013). We have no sedimentological or stable isotope evidence for low oxygen conditions, and $CaCO_3$% remains high over the studied interval (Riesselman et al., 2007). Therefore, we interpret a high relative abundance of the infaunal, triserial buliminids as indicative of a high, year-round food supply (Jorissen et al., 1995, 2007; Gooday, 2003). High relative abundances of phytodetritus-using taxa indicate an overall more moderate, as well as highly fluctuating (seasonally or episodically) flux of non-refractory particulate organic matter (e.g. Gooday, 2003; Jorissen et al., 2007). A high relative abundance of *Nuttallides umbonifera* indicates waters highly corrosive to $CaCO_3$ in generally low-food supply settings (Bremer and Lohmann, 1982; Gooday, 2003).

Comparisons between past and recent benthic assemblages as indicators for features of deep-sea environments need careful evaluation, because Eocene deep-sea benthic foraminiferal assemblages were structured very differently from those living today, and the ecology even of living species is not well known. For instance, in the Paleogene, taxa reflecting highly seasonal or episodic

deposition of organic matter (phytodetritus) were generally absent or rare, increasing in relative abundance during the EOT (e.g. Thomas and Gooday, 1996; Thomas, 2007). At Walvis Ridge, these species did occur at much lower abundances during the EOT after Eocene hyperthermal event 2 (Jennions et al., 2015), during the transition from early into middle Eocene (Ortiz and Thomas, 2015) and during the middle Eocene climatic optimum (MECO; Boscolo-Galazzo et al., 2015). During the time interval from the early-late Eocene through the EOT their abundance thus increased overall, though episodically and with considerable fluctuations.

In contrast, in the Paleogene cylindrically-shaped taxa with complex apertures (called 'Extinction Group'-taxa by Hayward et al., 2012) were common (e.g. Thomas, 2007). These taxa globally declined in abundance during the increased glaciation of the earliest Oligocene and middle Miocene to become extinct during the middle Pleistocene (Hayward et al., 2012). The geographic distribution of these extinct taxa resembles that of buliminids but differs in detail (e.g. Hayward et al., 2012). These taxa were probably infaunal, as confirmed by their $\delta^{13}C$ values (Mancin et al., 2013). It is under debate what caused their Pleistocene extinction and decline in abundance across the EOB (Hayward et al., 2012; Mancin et al., 2013). Changes in the composition of phytoplankton, their food source, have been mentioned as a possible cause, as well as declining temperatures, increased oxygenation or viral infections (Hayward et al., 2012; Mancin et al., 2013).

2.4 Statistical treatment of the nannofossil data

Relative species abundances are commonly lognormally distributed (MacArthur, 1960). To generate suitable datasets for statistical analysis, different transformations yielding Gaussian distributions must be applied, such as log transformation (e.g. Persico and Villa, 2004; Saavedra-Pellitero et al., 2010), centered log-ratio (e.g. Kucera and Malmgren, 1998; Buccianti and Esposito, 2004), arcsine (e.g. Auer et al., 2014).

The nannofossil species percentages were used in the statistical treatment to compare the datasets A and B. Two transformations were tested: i) log-transformation by log(x+1), which amplifies the importance of less abundant species, and minimizes the dominance of few abundant species (Mix et al., 1999), and ii) centered log-ratio (clr) transformation (Aitchison, 1986; Hammer and Harper, 2006), which opens a closed data matrix and retains the true covariance structure of compositional data. The normal distribution of each species before and after the transformations was verified using SYSTAT 13.0 software. Datasets A and B were treated the same, but analysed independently.

Principal component analysis (PCA) was performed on the transformed data using the statistics software PAST (PAleontological STatistic; Hammer et al., 2001). Species with an abundance <1% in all samples were not included in the PCA. The PCA (Q-mode) was performed to identify the major loading species and to evaluate the main factors affecting the changes on fossil coccolithophore assemblages.

The closed-sum problem, or constant-sum constraint, may obscure true relationships among variables (Pearson, 1896). The clr transformation retains a major problem in carrying out the PCA on the covariance matrix, and the goal of keeping the most important data information with only few principal components (PCs) can fail using clr transformation in associations containing many outliers (e.g. Maronna et al., 2006), as often the case in nannofossil assemblages. To minimize the presence of outliers we worked with abundant species and groups of nannofossils, instead of with single species.

The PAST software was also used to calculate the Shannon Index, H, a diversity index taking into account a combination of evenness and diversity. High values indicate high evenness and/or high richness.

3 Biostratigraphy

The EOB at Site 1263 was tentatively placed between 83 and 110 mcd by the Leg 208 Shipboard Scientific Party (Zachos et al., 2004). Our high-resolution sampling allowed refining the position of the EOB by locating nannofossil and planktonic foraminiferal bioevents (Fig. 2; Table 1), including some bioevents not reported in Zachos et al. (2004).

The identified bioevents are delineated as Base (stratigraphic lowest occurrence of a taxon), Top (stratigraphic highest occurrence of a taxon), and Base common (Bc, first continuous and relatively common occurrence of a taxon) following Agnini et al. (2014). No correlation with magnetochrons was possible because the nannofossil oozes did not carry a clear signal (Zachos et al., 2004). The depths of all identified nannofossil and planktonic foraminiferal datums, together with the ages assigned to the most reliable datums as defined in Pälike et al. (2006) and Gradstein et al. (2012) are displayed in Table 1. Only one bioevent - the Top of *Isthmolithus recurvus* - is not reported in Pälike et al. (2006): thus, we adopted the age given in Lyle et al. (2002) (Table 1).

Based on the identified bioevents (see below for details), we documented that the studied succession spans from 32.7 Ma (Top of *I. recurvus*, Lyle et al., 2002) to 34.77 Ma (Top of *Discoaster barbadiensis*, Pälike et al., 2006). The estimated average sedimentation rate is 12

337 m/myr, close to the average value of ~10.8 m/myr in Zachos et al. (2004). In dataset A, where the
338 sample distribution is more homogeneous, the sampling resolution is <10.000 years across the EOT
339 (from 97.29 to 90.02 mcd).

340

341 **3.1 Calcareous nannofossils**

342 The results from both datasets A (higher-resolution) and B (longer time interval) render similar
343 biostratigraphical evidence and well-constrained bioevents, especially for the rare species. Using
344 the absolute (N g^{-1}) and relative (%) abundances of both datasets, we identified nine calcareous
345 nannofossil datums (Fig. 2; Table 1). The studied interval spans from CNE20 (pars) Zone to CNO2
346 (pars) Zone, in the recent biozonation of Agnini et al. (2014). The bioevents include:

347 • Base of *Sphenolithus tribulosus*, the lowermost datum identified (at 103.11 mcd, Table 1). We
348 detected this species at the top of CNE20 Zone (Fig. 2), slightly below the range reported by
349 Bown and Dunkley Jones (2006), who documented it between the NP21 and NP23 Zones
350 (biozonation of Martini, 1971) corresponding to the CNE21-CNO4 Zones (Agnini et al., 2014).
351 At Site 1263, this species is rare and sporadic and poor preservation of the studied material
352 compromises the identification at the species level and thus, possibly, its Base.
353 • Top of *Discoaster barbadiensis* and *Discoaster saipanensis*. The rosette-shaped discoasters at
354 the bottom of the succession are usually well preserved without overgrowth (Fig. S1,
355 Supplement). The Top of *D. barbadiensis* was not reported by the Shipboard Scientific Party
356 (Zachos et al., 2004), and we placed this bioevent one meter below the Top of *D. saipanensis*
357 (Fig. 2), identified by Zachos et al. (2004) two meters below our datum (Table 1). We placed the
358 Top of *D. saipanensis* at 102.27 mcd because specimens of *D. saipanensis* had been
359 continuously found until 102.52 mcd, although outside the count of 300 specimens (Fig. 2).
360 These two bioevents were usually considered concurrent, but high-resolution studies (Berggren
361 et al., 1995; Lyle et al., 2002; Tori, 2008; Blaj et al., 2009; Fioroni et al., 2015) show that they
362 are shortly spaced. The Top of *D. saipanensis* is used to define the CNE20/21 zonal boundary.
363 • Base common of *Clausicoccus subdistichus*. We included *Clausicoccus obrutus* in the *C.*
364 *subdistichus* concept following Agnini et al. (2014), although *C. obrutus* is the most abundant of
365 the two species at Site 1263 (see Fig. S2, Supplement). The absolute abundance variations
366 together with the relative abundance in the more detailed dataset A, identify the Bc at 96.92 mcd,
367 ~2 m below the depth reported by the Leg 208 Shipboard Scientific Party (94.77 mcd; Table 1;
368 Fig. 2) and ~60 cm above the observed Top of *Hantkenina* spp. and reduction in size of
369 *Pseudohastigerina* (Fig. 2; see the foraminifer section). The Bc of *C. subdistichus* defines the

base of CNO1 (Agnini et al., 2014), which corresponds to the upper zone NP21 (Martini, 1971). The Bc of *C. subdistichus* (referred to as *C. obruta*) has been observed shortly after the EOB at Deep Sea Drilling Project (DSDP) Sites 522 and 523 in the SE Atlantic (Backman, 1987) - in the vicinity of Site 1263 - as well as in the Tethys Massignano GSSP and Monte Cagnero sections (Tori, 2008; Hyland et al., 2009), at high-latitude Site 1090 (Marino and Flores, 2002) and in the NW Atlantic (Norris et al., 2014).

- Base of *Chiasmolithus altus*. The rare and discontinuous presence of *C. altus* creates some bias in the detection of its Base. Moreover, *C. altus* specimens are highly affected by dissolution as their central-area is commonly completely dissolved (Fig. S1, Supplement). The Base of *C. altus* is tentatively placed at 89.4 mcd where a specimen with whole central crossbars meeting at 90° was observed (Fig. S1, Supplement). At Site 1263, the Base of *C. altus*, the youngest representative of the genus, falls inside the lower Oligocene (Zone CNO1; Fig. 2), as also documented NE Atlantic (de Kaenel and Villa, 1996) and at high-latitudes (Persico and Villa, 2004; Villa et al., 2008).
- Base and Bc of *Sphenolithus akropodus*. Rare sporadic occurrence and poor preservation affect the recognition of this species, but Bc was identifiable (Fig. 2; Table 1). We tentatively placed the Base also, but just few and sporadic species were detected (Fig. 2). The Bc is consistent with the identified datum reported in de Kaenel and Villa (1996), who used this bioevent to approximate the Zone NP21/22 boundary, and the Top of *Coccolithus formosus*.
- Top of *Coccolithus formosus*. This bioevent was easily detectable, as *C. formosus* is abundant and well preserved. Its Top defines the CNO1/CNO2 zonal boundary (Fig. 2), close to the depth suggested on board ship (Table 1).
- Top of *Isthmolithus recurvus*, the highest datum identified (Fig. 2). Its abundance is low, so that its distribution becomes discontinuous towards the top of the studied interval. The 83.19 mcd depth (Table 1), 3 m above that reported by the Shipboard Scientific Party (Zachos et al., 2004), is an approximation because just one sample above the highest observed specimens of *I. recurvus* was analysed.

3.2 Planktonic foraminifers

The Eocene-Oligocene boundary (EOB; ~33.89 Ma, Gradstein et al., 2012) is denoted at its Global Stratotype Section and Point (GSSP) at Massignano in Italy by the extinction of the Family Hantkeninidae (specifically of species in the genera *Hantkenina* and *Cribrohantkenina*; Premoli Silva and Jenkins, 1993). Unless well-preserved material is available (as for e.g. the Tanzania

403 Drilling Project (TDP) sites; Pearson et al., 2008), the sensitivity of hantkeninids to fragmentation
404 and dissolution may lead to a misplacement of its true highest occurrence. At several well-studied
405 sites, for example ODP Site 744 (Zachos et al., 1996) and Site 1218 (Coxall et al., 2005),
406 hantkeninids are not present. In such cases, additional planktonic foraminifer bioevents must be
407 considered to identify and correlate the EOB between sites: i) the extinction of the *Turborotalia*
408 *cerroazulensis* group which preceded the EOB (Berggren and Pearson, 2005; Pearson et al., 2008),
409 and ii) the reduction in size of the *Pseudohastigerina* lineage which occurred at the EOB (Wade and
410 Pearson, 2008 and references therein).

411 At Site 1263, planktonic foraminifers are abundant and their preservation is generally good to
412 moderate. Samples from 109.79 to 99.97 mcd, however, contain strongly fragmented planktonic
413 foraminifers, with non-broken specimens dominated by heavily calcified *Globigerinatheca* spp.
414 (Zachos et al., 2004). Unfortunately, species of the hantkeninid group are not well preserved, and
415 occur as fragments of variable size, including tubulospines and partial specimens (several
416 chambers). Entire or partially preserved specimens of hantkeninids as well as loose tubulospines
417 have been observed from the bottom sample (107.29 mcd) up to 97.91 mcd. No specimen of
418 *Hantkenina* spp. nor even tubulospine were seen from 97.14 mcd upward (Table S1, Supplement).
419 Therefore, we focused on the Top of *T. cerroazulensis* group (comprising *T. cerroazulensis*, *T.*
420 *cocoaensis*, and *T. cunialensis*) and the size reduction of the *Pseudohastigerina* lineage,
421 characterized as the Top of >125 µm-sized *Pseudohastigerina micra*. These two bioevents where
422 detected at the same depth as the Top of *Hantkenina* spp., i.e. the three bioevents all fall in between
423 97.91 and 97.14 mcd (Fig. 2; Table S1, Supplement). Due to the lower resolution of the sampling
424 for planktonic foraminifers than for nannofossils, the three bioevents may not be exactly coeval, but
425 occur with that interval of less than 1 meter (~70 kyr). Nevertheless, we can refine the position of
426 the EOB reported in Zachos et al. (2004), where only core catcher samples were studied, and place
427 the EOB between 97.91 and 97.14 mcd, i.e. at 97.53 mcd (Fig. 2). This position of the EOB is in
428 agreement with the nannofossil bioevent, Bc of *C. subdistichus*, just above that level (96.92 mcd;
429 see Section 3.1).

430 A further confirmation of this placement of the EOB comes from the benthic foraminifer oxygen
431 isotope data. The EOB occurs between the two main steps in $\delta^{18}O$ characterizing the EOT cooling
432 and glaciation at TDP Sites 12 and 17, where assemblage are pristine (Pearson et al., 2008). At Site
433 1263, high resolution $\delta^{18}O$ data are available only from 96 mcd up. Step 2 is identifiable at 93.4
434 mcd, at the maximum value of benthic $\delta^{18}O$ (Fig., 2; Riesselman et al., 2007; Peck et al., 2010).
435 Step 1 was tentatively placed by Peck et al. (2010) at ~93.8 mcd, but the $\delta^{18}O$ curve does not reveal
436 a signal of the first cooling step as clear as at Pacific Site 1218 (Coxall et al., 2005) and nearby Site

522 at Walvis Ridge (Zachos et al., 1996; Coxall and Wilson, 2011). We argue that Step 1 should be placed below 97.53 mcd at Site 1263, not only on the basis of the planktonic foraminiferal and nannofossil bioevents, but also by comparison with the oxygen isotope curve at Site 522, which records a complete and clear $\delta^{18}O$ signal for the entire EOT (Fig. 2). The two sites are geographically close, and have comparable sedimentation rate across the EOT (12 m/myr at Site 1263; 9 m/myr at Site 522, Hsü et al., 1984). Because Step 1 and Step 2 occur within ~4 meters at Site 522 (Zachos et al., 1996; Coxall and Wilson, 2011), we can infer that a similar pattern is present at Site 1263, placing the Step 1 between 97.5 and 98.5 mcd (Fig. 2). A $\delta^{18}O$ signal similar to the one at Site 522, with Step 1 placed ~2 meters below the EOB, is recorded at Site 1265 on the Walvis Ridge (lower sampling resolution; sedimentation rate 5.7 m/myr; Liu et al., 2004). These evidences do not agree with the previous proposed position for Step 1 at only 40 cm below Step 2 (Peck et al., 2010). More oxygen isotope analyses are necessary to definitely place Step 1 in the sediment column at Site 1263.

4 Biotic responses

4.1 Calcareous nannofossil preservation and assemblages

At ODP Site 1263 the carbonate content did not increase above the EOB (Fig. 3; Riesselman et al., 2007), in contrast to other sites, specifically in the Pacific Ocean (e.g. Salamy and Zachos, 1999; Coxall et al., 2005; Coxall and Wilson, 2011). This lack of response is probably due to the location of Site 1263 well above the lysocline since the late Eocene (Zachos et al., 2004), so that $CaCO_3$ (wt%) was and remained generally high, and was not affected by CCD deepening (Fig. 3; Riesselman et al., 2007). The deeper Site 1262, close to Site 1263, was below the lysocline before the rise in CCD, and shows a strong increase in $CaCO_3$ (wt%) across the EOB (from ~5 to > 90%; Liu et al., 2004).

However, the $CaCO_3$ (wt%) at Site 1263 does not reflect the total coccolith absolute abundance (Fig. 3). This supports that other calcifying organisms (mainly planktonic foraminifers) contributed consistently to the calcite accumulation in the sediments. To unravel the "true" contribution of each calcifying group to the accumulated $CaCO_3$ (wt%), we need to know the total amount of carbonate produced by calcareous nannoplankton and foraminifers, which is beyond the scope of this study.

Although the site was above the lysocline during the studied time interval, the nannofossil and foraminiferal assemblages show signs of dissolution throughout the sequence. Dissolution may occur above the lysocline (e.g. Adler et al., 2001; de Villiers, 2005), leading to a reduction in

species numbers and an increase of fragmentation with depth, in both nannoplankton (e.g. Berger, 1973; Milliman et al., 1999; Gibbs et al., 2004) and planktonic foraminiferal assemblages (e.g. Peterson and Prell, 1985).

At Site 1263 signs of dissolution were detected, in particular, in specimens of *Cyclicargolithus* (Fig. S1, Supplement) – one of the least resistant nannoplankton species (Blaj et al., 2009), but also in more robust species such as *Dictyococcites bisectus*. Despite these signs, holococcoliths and abundant small-medium sized *Cyclicargolithus* – which are prone to dissolution (Young et al., 2005; Bown et al., 2008; Blaj et al., 2009) – are present in all samples. We did not see small placoliths (<3 μm) at Site 1263, possibly due to dissolution, but these were not dominant in the late Eocene (e.g. Persico and Villa, 2004; Villa et al., 2008; Fioroni et al., 2015). The lack of such placoliths does not prevent the identification of the main features of the medium-large sized taxa.

Our coccolith dissolution index does not show any major changes across the EOT (91-98.5 mcd), but at 90.2 mcd and from 87 mcd upward nannofossil dissolution slightly increased (Fig. 3). The correlation between the dissolution index and total coccolith abundance is positive (entire interval r = 0.32; *p*-value = 0) and stronger in the upper interval of the studied sequence (r = 0.59; *p*-value = 0.002), but not significant across the EOB. Intervals of increased dissolution do not necessarily correspond to lower absolute abundances, so that we can infer that primary signals of the nannoplankton are preserved in the fossil assemblages at least across the EOB, with the exception of the primary presence/absence of small specimens.

Nannofossil diversity, as expressed in the H index, does not vary significantly across the EOB, but decrease gradually within 1.5 m above the EOB. A more distinct step-wise decrease at 90 mcd (Fig. 3) reflects a community structure with fewer dominant species, possibly due to increased dissolution in this interval, and by a community structure with fewer dominant species. Actually, *Cyclicargolithus* became dominant in this interval, while large *Reticulofenestra* decreased in abundance significantly (Fig. 3). The calcareous nannofossil assemblage variations recorded in sample sets A and B are comparable despite the different sampling resolution (Figs. S2 and S3, Supplement).The trends in absolute and relative abundances are very similar (Fig. S2, Supplement). Thus, we conclude that the dilution/sedimentation rates at Site 1263 were close to constant over time, and that the variations in absolute abundance were linked to biological processes. Total absolute coccolith abundances show a marked decrease ~1.5 m above the EOB (Fig. 3): within 60 cm (from 96.39 to 95.79 mcd) the abundance rapidly drops by 45%, mainly driven by the loss of large-sized species, including *D. bisectus*, *Dictyococcites stavensis*, *Reticulofenestra umbilicus*, *Reticulofenestra samodurovii*, *Reticulofenestra hillae*, and *Reticulofenestra circus* group (see

taxonomical remarks in the Supplement). Among these, *D. bisectus* and *D. stavensis* constitute a significant part (up to 28%) of the assemblage. The medium-sized *Reticulofenestra daviesii* also shows a decrease ~1.5 m above the EOB, contrary to what was reported at ODP Site 744 (Persico and Villa, 2004), Site 748 (Villa et al., 2008), Site 711 (Fioroni et al., 2015), and Site 1090 (Pea, 2010) for the same time interval. The small-medium *Cyclicargolithus* spp. and *C. floridanus* are the most abundant species (up to 50%), and the 5-7 μm size group is dominant. This group increases slightly from the bottom upwards, and just above the EOB it records an increase in abundance. *Coccolithus pelagicus* is another important component of the nannofossil assemblage, at a maximum abundance of 27% (Fig. 3). This species increases in abundance between 96.92-92.6 mcd, i.e. above the EOB, and then it decreases from 88 mcd upwards. *Sphenolithus* spp. does not show any marked variation at the EOB, even if this group is not very abundant. The increase of *Cyclicargolithus* and *C. pelagicus* does not coincide with the marked decrease of large reticulofenenstrids indicating that the loss of the latter group was not compensated for by other taxa. The total coccolith abundance (and export production) thus decreased above the EOB.

Another component of the assemblage, *Lanternithus minutus*, is generally not abundant, but peaks between 89.6 and 87.12 mcd. *Zygrablithus bijugatus* and *Discoaster* spp. both decreased in abundance below the EOB (at 98 and 99 mcd, respectively) and higher in the section never reached abundances as high as in the upper Eocene (Fig. 3).

4.1.1 Principal component analysis

Results from the PCAs performed on datasets A and B are comparable, both using the log- or clr-transformation. For dataset A, the Pearson correlation value (r) between the components from the two transformations is 0.90 (*p*-value=0), confirming that the primary signals in the assemblage are reflected in the multivariate statistical analysis, as long as normal distribution of the species is maintained. We also compared the PCA results with or without the presence of the marker species, because stratigraphically-controlled species are not distributed along the entire succession, thus affecting PCA outcomes (e.g. Persico and Villa, 2004; Maiorano et al., 2013). The results obtained with and without the marker species provide similar trends for both datasets because in the studied interval the marker species are not very abundant (Fig. 4; Table S2, Supplement).

In the following discussion, we will focus on the PCA results and the loading species using the log-transformation for datasets A and B (Fig. 4; Tables S2 and S3, Supplement). The only two significant principal components explain 50% of the total variance in dataset A, and respectively

account for 36% and 14%. For dataset B the two components explain 35% (26% and 11% respectively).

Principal component 1 (PC1) of dataset A shows positive values below 96 mcd. A pronounced decrease occurs 1.5 m above the EOB, and from 96 mcd upwards the PC1 maintains mainly negative values (Fig. 4a). PC1 is negatively loaded by *C. obrutus*, *C. floridanus* small and medium size, and positively by *D. stavensis*, *D. bisectus*, *R. daviesii*, and *R. umbilicus* (Fig. 4a; Table S2, Supplement). The loadings of the other species are too low to be significant. The PC1 of dataset B does not record the same marked drop above the boundary, but rather a gradual decrease along the whole sequence (Fig. 4a). Although the main loading species are the same for both datasets (i.e. *C. obrutus*, *Cyclicargolithus* versus *D. bisectus* and *R. umbilicus*), there are some differences (Tables S2 and S3, Supplement). Specifically, the size groups of *Cyclicargolithus* do not influence PC1 in dataset B because the size subdivision was not included in the counts of that dataset. As the distribution of large *versus* small-medium sized species on the PCA seems to be important for both datasets, and *Cyclicargolithus* is one of the most abundant species, the lack of a detailed size grouping within this genus in dataset B might be the cause of the difference in the PC1 curves above the EOB. The higher abundances of *Discoaster* and *R. umbilicus* from the bottom up to 102 mcd in dataset B could also explain some differences in the loading species between the two datasets (Tables S2 and S3, and Fig. S3, Supplement).

Principal component 2 (PC2) of dataset A also records an abrupt variation above the EOB (at 96 mcd): the negative values at the bottom of the succession turn toward positive values above the boundary, remaining positive up to 89.95 mcd. From 90 mcd upwards, PC2 displays mainly negative values, except for a peak between 85.68-86.42 mcd (Fig. 4b). The most meaningful species loading on PC2 is *L. minutus* (negative loading). The PC2 is also loaded negatively by *D. stavensis* and *C. floridanus* (5-7 µm), and positively by *C. pelagicus* (3-7 µm and 7-11 µm), *I. recurvus* and *Sphenolithus* spp. (Fig. 4b; Table S2, Supplement). The PC2 for dataset B shows a trend similar to that for dataset A from 98 mcd upward (Fig. 4b), but it distinctly differs in the lower part of the succession. Again, the PC2 is resolved by the same main loading species *L. minutus* versus *C. pelagicus*, but the relative direction (positive or negative) of the loadings is reversed between datasets A and B (Tables S2 and S3, Supplement). In particular, *L. minutus* has very strong loadings in both datasets. In dataset B, *L. minutus* has its maximum abundance in the upper Eocene interval not sampled in dataset A (Figs. S2 and S3, Supplement), likely driving the differences between the two PC2 curves below the EOB (Fig. 4b).

In the following discussion, we used the PCA results for dataset A (without marker species) only, because of its more even sample distribution and direct comparison to the other available nannofossil proxies, i.e. dissolution index, coccolith size distribution and absolute abundance.

4.2 Mean coccolithophore cell size variations

The PC1 curve is mirrored (r=0.79; *p*-value=0) by mean cell size estimates (V:SA ratio) of all medium to large-sized (>3 µm) placolith-bearing coccolithophores within the assemblages and of those all ancient alkenone producers combined (i.e. *Cyclicargolithus*, *Reticulofenestra* and *Dictyococcites*; Plancq et al., 2012) (Fig. 5). Fluctuations in mean size are mainly driven by the relative abundance of the different placolith-bearing taxa and their respective size groups, rather than by intra-specific size variations. The mean V:SA ratios were higher (species with large cells were more abundant) during the latest Eocene and early Oligocene, and the size decreased (due to the loss of large species) by 8% between 96.39 to 95.79 mcd (within ~47 kyr), which is according to our age model ~120 kyr after the EOB.

The coccolith dissolution index confirms that preferential dissolution did not bias the V:SA results, as intervals of increased dissolution did not generally correspond to large V:SA (r = -0.12). The only exception is the top, 90-90.3 mcd, interval where a high dissolution peak corresponds to an increase in mean size. In either case, the above V:SA considerations do not include small placoliths (<3 µm), so that our analysis is free from any bias due to the (original) presence or absence of this most dissolution-prone group.

4.3 Benthic foraminiferal assemblage

Benthic foraminifers show partial dissolution or etching, especially between 94.42 mcd and 109.79 mcd, but are generally well preserved, i.e. sufficient for determination at species level (Fenero et al., 2010). The low-resolution data on benthic foraminifers show that the diversity of the assemblages (Fisher's alpha index curve; Fig. 6) started to decline in the late Eocene (~34.5 Ma; 102.79 mcd), reached its lowest values just below the EOB, then slowly recovered, but never to its Eocene values (Fenero et al., 2010). The decline in diversity was due in part to a decline in relative abundance of the generally rare but species-rich group of rectilinear species with complex apertures ('extinction group' species). Such a decline is observed globally at the end of the Eocene (Thomas, 2007; Hayward et al., 2012). The declining diversity (decreased evenness) was also due to a transient increase in abundance of species indicative of seasonal delivery of food to the sea floor

(phytodetritus species, mainly *Epistominella* spp.; ~33.9-33.4 Ma; 97.91-91.91 mcd), with a short peak in overall, year-round food delivery above the EOB (buliminid taxa; ~33.8 Ma; 96.41-96.27 mcd). From ~3 meter above Step 2 (~33.3 Ma; 90.41 mcd) up, the abundance of *N. umbonifera*, an indicator of carbonate corrosive bottom waters, increased. Due to this evidence for dissolution, benthic foraminiferal accumulation rates cannot be used to estimate food supply quantitatively and reliably throughout the studied interval.

Evidence for effects of dissolution on benthic foraminiferal assemblages is seen in the interval where *N. umbonifera* is common, but not in the interval with peak abundance of phytodetritus species (thin-walled, solution-sensitive species), and the interval where buliminids peak. These intervals are also not recognized as influenced by carbonate corrosivity in the pore waters (Riesselman et al., 2007). Thus, we conclude that the increased percentage of infaunal taxa is, in this studied section, not due to dissolution, although such an effect is seen in sections with much more severe dissolution effects, such as the Paleocene-Eocene interval of ocean acidification (Foster et al., 2013). Increased abundance of buliminid taxa (though not of phytodetritus taxa) could possibly result from lowered oxygen conditions in bottom or pore waters (e.g. Jorissen et al., 2007). However, there are no indications in the sediment of low oxygen conditions (e.g. lamination), and the overall benthic assemblage does not indicate low oxygen conditions (e.g. the diversity is too high).

5 Discussion

5.1 Nannoplankton abundance and cell size decrease after the EOB

The distinct variation in nannoplankton abundance and average size of medium to large placoliths above the EOB at Site 1263 cannot be explained by dissolution – which would affect smaller coccoliths preferentially and lead to an increase of the mean size of the whole assemblage, opposite to what is observed. It can also not be explained by a change in species diversity, but is mainly linked to changes in community structure (Fig. 3). The drop in total nannofossil abundance (Fig. 3) and mean cell size (Fig. 5) is mainly driven by the decrease in abundance of large *Reticulofenestra* and *Dictyococcites* 1.5 m (~120 kyr) above the EOB. The mean V:SA estimates for all ancient alkenone producers combined (i.e. *Cyclicargolithus*, *Reticulofenestra* and *Dictyococcites*; Plancq et al., 2012) tightly overlap (Fig. 5) with biometric data of the same group in the Equatorial Atlantic (Ceara Rise, ODP Sites 925 and 929; Pagani et al., 2011; Zhang et al., 2013), while the mean size estimates for combined *Reticulofenestra* and *Dictyococcites* remained relatively stable and coincide

630 with mean values measured at ODP Site 1090 in the Subantarctic Atlantic, where *Cyclicargolithus*
631 spp. were not present and assemblages are likely severely affected by dissolution (Pea, 2010; Pagani
632 et al., 2011). This highlights that the observed patterns in average placolith size at Site 1263 are
633 driven by the decrease in abundance, rather than (intra-specific) size variations of *Reticulofenestra*
634 and *Dictyococcites*.

635 The assemblages also illustrate the mid-latitude location of Site 1263, hosting both "subantarctic"
636 and "equatorial" taxa. A striking correspondence between the mean V:SA of ancient alkenone
637 producers at Site 1263 and Sites 929 and 925 (Fig. 5) would suggest more affinity with tropical
638 assemblages than with high-latitude ones, south of the Subtropical Convergence (STF). The
639 abundance patterns of the larger reticulofenestrids, however, are more similar to those at Southern
640 Ocean sites (Persico and Villa, 2004; Villa et al., 2008). The mid-latitudinal Site 1263 thus probably
641 records paleobiogeographic patterns in the nannofossil assemblage intermediate between those in
642 equatorial-tropical and subantarctic regions.

643 The coccolith size-shift and the decreased abundance of large reticulofenestrids after the EOB may
644 be related to different bio-limiting factors. Under growth-limiting environmental conditions,
645 phytoplankton (coccolithophores) with small cell volume-to-surface area ratios may outcompetes
646 larger cells due to lower resource requirements (lower C, P and N cell quota) and generally higher
647 growth rates (e.g. Daniels et al., 2014). A change in overall nutrient regime, such as in coastal
648 upwelling *versus* oligotrophic, stratified gyre systems, may also cause a shift in opportunistic *versus*
649 specialist taxa (e.g. Falkowski et al., 2004; Dunkley Jones et al., 2008; Henderiks et al., 2012). The
650 16-37% absolute abundance declines of the reticulofenestrid species *R. umbilicus*, *R. samodurovii*
651 *R. hillae* and *R. circus* group (Figs. 3 and S2, Supplement), are strong indications that these large-
652 celled coccolithophores were at a competitive disadvantage already during or shortly after the EOB.
653 Earlier biometric studies of reticulofenestrid coccoliths point to a similar scenario (Fig. 5),
654 postulating that the macroevolutionary size decrease reflects the long-term decline in pCO_2
655 (Henderiks and Pagani, 2008; Pagani et al. 2011; Hannisdal et al., 2012). High CO_2 availability
656 during the late Eocene could have supported high diffusive CO_2-uptake rates and photosynthesis
657 even in the largest cells, assuming that Paleogene coccolithophores had no or inefficient CO_2-
658 concentrating mechanism, similar to modern species today (Rost et al., 2003; Bolton and Stoll,
659 2013), and due to the fact that RUBISCO specificity for CO_2 increases at higher CO_2 levels
660 (Giordano et al., 2005).

661 Available paleo-pCO_2 proxy reconstructions from Equatorial regions (Pearson et al., 2009; Pagani
662 et al., 2011; Zhang et al., 2013) indicate a transient decrease in pCO_2 across the studied interval,

663 rather than a distinct drop in pCO_2 after the EOB, which appears to be supported by our high-
664 resolution assemblage (PC1) and mean V:SA time series (Fig. 5). The paleo-pCO_2 proxy data,
665 however, are at much lower time resolution, based on a range of geochemical proxies and
666 assumptions (Pearson et al., 2009; Pagani et al., 2011; Zhang et al., 2013). Therefore they may not
667 record the drop in pCO_2 as accurately as our comparative analysis would require. The range of
668 estimated pCO_2 values is fairly wide: mean values are 940 ppmv before the EOB (standard
669 deviation range 740-1260 ppmv) and 780 ppmv after the boundary (s.d. range 530-1230 ppmv)
670 (Pearson et al., 2009; Pagani et al., 2011; Zhang et al., 2013; Fig. 5).

671 Possibly, shortly after the EOB a threshold level in pCO_2 was reached, below which large
672 reticulofenestrids became limited in their diffusive CO_2-uptake, or other, fast-changing (a)biotic
673 environmental factors limited the ecological success of this group. On million-year time scales,
674 atmospheric CO_2 levels appear to have influenced coccolithophore macroevolution more than
675 related long-term changes in temperature, sea level, ocean circulation or global carbon cycling
676 (Hannisdal et al., 2012). Between biotic and abiotic factors, the latter (i.e. nutrient supply,
677 temperature, salinity, etc.) are deemed to be dominant (Benton, 2009), and may have led to a more
678 successful adaptation of the smaller taxa at the expense of large ones (see discussion below, Section
679 5.2).

680 This would not exclude a transient, long-term pCO_2 forcing on coccolithophore evolution
681 (Hannisdal et al., 2012). Interestingly, the decline of large *R. umbilicus* occurred earlier at Site 1263
682 (~33.8 Ma) than at higher latitudes in the Southern Ocean (~33.3 Ma at Site 689, Persico and Villa,
683 2004; ~33.5 Ma at Site 748, Villa et al., 2008). A similar pattern is documented in the timing of its
684 subsequent extinction, occurring earlier at low- and mid-latitudes (32.02 Ma; Pälike et al., 2006)
685 and later at high latitudes (31.35 Ma; Gradstein et al., 2012). Henderiks and Pagani (2008)
686 suggested that the generally higher content of CO_2 in polar waters may have sustained *R. umbilicus*
687 populations after it had long disappeared from the tropics.

688

689 **5.2 Paleoproductivity at Site 1263: nannoplankton and benthic foraminifer signals**

690 At Site 1263, no other phytoplankton than calcareous nannoplankton was detected, and diatoms
691 were absent in coeval sediments at near-by DSDP Walvis Ridge Sites 522-529 (Hsü et al., 1984;
692 Moore et al., 1984). Therefore, our inferences of paleo-primary productivity and export production
693 are based on the nannoplankton and benthic foraminiferal assemblages.

PC2 of the calcareous nannoplankton analysis could be correlated with paleoproductivity and total water column stratification. The strongest negative loading on PC2 is the holococcolith *L. minutus* (Fig. 4b; Table S1, Supplement). In modern phytoplankton, the holococcolith-bearing life stages proliferate under oligotrophic conditions (e.g. Winter et al., 1994). Moreover, holococcoliths such as *L. minutus* and *Z. bijugatus* are quite robust (Dunkley Jones et al., 2008), so that dissolution is unlikely to affect their distribution.

The positive loadings on PC2 are the species *C. pelagicus*, *I. recurvus* and *Sphenolithus* spp. A high abundance of *C. pelagicus* has often been considered as indicative for warm-to-temperate temperatures at high-latitudes (e.g. Wei and Wise, 1990; Persico and Villa, 2004; Villa et al., 2008). In the modern oceans, *C. pelagicus* seems to be restricted to temperate-to-cool water, high-nutrient conditions (e.g. Cachao and Moita, 2000; Boeckel et al., 2006), but during the Paleogene it was cosmopolitan (Haq and Lohmann, 1976). The paleoecological preferences of *Sphenolithus* are still controversial, but it has been related to oligotrophic conditions inferring a major nutrient control rather than temperature control on this species during the Paleocene-Eocene thermal maximum (PETM; Agnini et al., 2006) and the EOT (Villa et al., 2008). Increased abundances of *Sphenolithus* have been also related to high-productivity intervals in the early Oligocene (Wade and Pälike, 2004) and across the EOT (Dunkley Jones et al., 2008).

We compared PC2 with the proxy for regional paleoproductivity $\Delta\delta^{13}C_{P\text{-}B}$ (Fig. 6), with lower values corresponding to lower productivity and/or higher stratification. $\Delta\delta^{13}C_{P\text{-}B}$ data are not available for the interval below 96 mcd (upper Eocene-lower Oligocene), but lower paleoproductivity in general corresponds to negative loadings on PC2, and vice versa. The correlation coefficient between the two curves is 0.33 (*p*-value =0.05), i.e. a significant but not very strong correlation, possibly due to the lower number of stable isotope data points than nannofossil data points. We infer that PC2 probably reflects lower productivity during the latest Eocene, with both PC2 and $\Delta\delta^{13}C_{P\text{-}B}$ curves showing higher productivity within the EOB and the onset of Step 2 (Fig. 6). In particular, PC2 records a longer interval of positive loadings (higher productivity) after the EOB, and an initial decrease corresponding to the highest peak in $\delta^{18}O$ (at~93 mcd; ~33.5 Ma), as recorded also by $\Delta\delta^{13}C_{P\text{-}B}$. According to the $\Delta\delta^{13}C_{P\text{-}B}$, paleoproductivity remained constant above 90 mcd upward, and lower than below Step 2. The different trend in PC2 from 90 mcd upward may be related to increased nannofossil dissolution, in particular above 87 mcd. The increase of dissolution is confirmed by the increased abundance of the benthic foraminifer species *N. umbonifera*, indicative of more corrosive bottom waters, and the intensified dissolution interval recorded by the coccolith dissolution index (compare Figs. 3 and 6).

727 The benthic foraminiferal assemblage confirms the above interpretation of the PC2, adding
728 information on the nature of the supply of organic matter to the seafloor, i.e. export productivity
729 (Fig. 6). The increase in abundance of the phytodetritus-using species across the EOB indicates an
730 increase in seasonality of food delivery to the seafloor, correlated to the interval with positive scores
731 on PC2 (Fig. 6). The interval was interrupted by a short period of increased productivity across the
732 EOB (as showed by the peak in the buliminid species curve at 96.27 mcd; Fig. 6), indicating high,
733 less seasonally interrupted food supply. Seafloor conditions changed after Step 2, when the high
734 abundance of *N. umbonifera* and the decrease of phytodetritus and buliminid species indicate more
735 corrosive bottom waters, possibly combined with less food arriving at the sea floor and a less
736 pronounced seasonality (Fig. 6).

737 Variations in nutrient supply to the photic zone, as reflected in nannofossil, is a factor that could
738 possibly have combined with the declining pCO_2 to cause the decrease in the mean coccolith size
739 after the EOB. The transient higher availability of nutrients between the EOB and the onset of Step
740 2 (~330 kyr), may have given small opportunistic nannoplankton species a competitive advantage
741 over large specialist species after this time. The decrease of mean cell size (less biomass per
742 individual) and overall decrease in nannofossil abundance could have led to less available organic
743 matter or less efficient ballasting of organic matter during transport to the sea floor and, less food
744 for the benthic foraminifers. If the smaller size led to decreased efficiency in ballasting, the time of
745 transport from surface to the sea floor could have increased, making remineralization more efficient
746 despite the declining temperatures. Ecosystem structure is the main determinant of efficiency of
747 transfer of organic matter to the sea floor (e.g. Henson et al., 2012), and such important changes as
748 observed in the nannofossil assemblages could have strongly impacted transfer of food to the
749 seafloor, hence benthic foraminiferal assemblages, and influenced the decline in 'Extinction Group'
750 species (Hayward et al., 2012; Mancin et al., 2013).

751 Possibly, climate-driven instability of the water column within 330 kyr after the EOB favoured
752 seasonal or episodic upwelling, thus primary productivity in this area, which may also be reflected
753 by the (slightly) increasing trends in absolute abundance of (medium-sized) *Cyclicargolithus* spp.,
754 *C. pelagicus* and *Sphenolithus* spp. (Fig. 3). After the major peak in $\delta^{18}O$ (Step 2) a more stable
755 system may have allowed the proliferation of more oligotrophic taxa, including holococcoliths, and
756 the establishment of more oligotrophic, stable environmental conditions (Fig. 6).

757 Previous studies documented an increase in primary productivity during the late Eocene-early
758 Oligocene, in particular in the Southern Ocean (e.g. Diester-Haass, 1995; Diester-Haass and Zahn,
759 1996; Salamy and Zachos, 1999; Persico and Villa, 2004; Schumacher and Lazarus, 2004;

760 Anderson and Delaney, 2005). At tropical latitudes, both transient increases (equatorial Atlantic;
761 Diester-Haass and Zachos, 2003) and decreases (e.g. Griffith et al., 2010; Moore et al., 2014) in
762 paleoproductivity have been recorded during the early Oligocene, with a sharp drop in the export
763 productivity during the early Oligocene at ~33.7 Ma (Moore et al., 2014), similar to what we
764 observed in the SE Atlantic. Schumacher and Lazarus (2004) did not record a significant shift of
765 paleoproductivity after the EOB in equatorial oceans, but noted a decrease in the early Oligocene
766 (after 31 Ma). An increase in seasonality after the EOB, similar to the one we recorded at mid-
767 latitudinal Site 1263, was documented at Site 689 in Southern Ocean (Schumacher and Lazarus,
768 2004), while seasonality increased just before Step 2 at northern high latitudes (Eldrett et al., 2009).

769

770 **5.3 Timing and possible causes of the biotic response at the EOB**

771 Marine faunal and floral extinctions and community changes were coeval with the climatic
772 deterioration during the late Eocene-early Oligocene (e.g. Adams et al., 1986; Coccioni, 1988;
773 Berggren and Pearson, 2005; Dunkley Jones et al., 2008; Pearson et al., 2008; Tori, 2008; Villa et
774 al., 2008, 2014). At ODP Site 1263, we see close correspondence between marked changes in the
775 nannoplankton assemblages (i.e. nannofossil abundance and coccolith size decrease) and the
776 benthic foraminiferal assemblages. The nannoplankton did not suffer significant extinctions at the
777 EOB as the planktonic foraminiferal assemblage did, but the change in the community was as fast
778 as extinction events (which occur within 10-100 kyr; Gibbs et al., 2005; Raffi et al., 2006), taking
779 place within ~47 kyr.

780 The main shifts in the nannoplanktonic community occurred during the EOT climatic transition,
781 ~250 kyr after the Step 1, and ~120 kyr after the EOB, but pre-dated the major cooling and increase
782 in Antarctic ice sheet volume (i.e. Step 2) by about 200 kyr. Therefore, nannofossil assemblages
783 prove to be sensitive and accurate tools to investigate climate thresholds and the early impacts of
784 climate change on biotic systems.

785 Benthic foraminiferal changes at Site 1263 started before the EOB, as observed at other sites
786 (Thomas, 1990, 2007), and the faunal turnover persisted into the early Oligocene. The benthic
787 faunas in general show a decline in abundance of rectilinear species with complex apertures,
788 possibly linked to the decline in nannoplankton species which they may have consumed (as e.g.
789 hypothesized by Hayward et al., 2012, Mancin et al., 2013). The increase in phytodetritus-using
790 species was possibly linked to more episodic upwelling and thus productivity and transport to the
791 sea floor, and potentially blooming of more opportunistic nannoplankton species. Unfortunately, the

792 lower resolution of the benthic foraminifer data compared to the nannofossil data does not allow to
793 unravel the exact timing of the benthic fauna response during the EOT, and also does not allow
794 exact correlation to changes in nannofossil assemblages.

795 At Site 1263 and in Southern Ocean records (Persico and Villa, 2004; Villa et al., 2008) the large
796 reticulofenestrids declined in abundance rapidly after the EOB. Persico and Villa (2004) and Villa
797 et al. (2008, 2014) inferred a strong influence of SST cooling on coccolithophores, and the drop in
798 SST shortly after the EOB at high-latitudes is confirmed by a decrease of 5°C in $U^{K'}_{37}$-based SST
799 (Liu et al., 2009). In contrast, at Site 1263 planktonic foraminifer Mg/Ca data record no significant
800 change in SST at that time (Peck et al., 2010; Fig. 5), as at ODP Sites 925 and 929 (tropical western
801 Atlantic) where $U^{K'}_{37}$-based SSTs show no significant cooling (Liu et al., 2009; Fig. 5). Fairly
802 stable SSTs were also documented in the tropics, using Mg/Ca-based SST reconstructions (Lear et
803 al., 2008). The temperatures at mid-latitudinal Site 1263 thus may have been stable, like those in the
804 tropics, rather than cooling, as inferred for high latitudes in the Southern Ocean (e.g. Persico and
805 Villa, 2004; Villa et al., 2008; Liu et al., 2009; Villa et al., 2014).

806 If this is true, SST may not have been the main environmental factor affecting the nannoplankton
807 assemblages at Site 1263 after the EOB. Andruleit et al. (2003) documented that temperature
808 changes may be of less importance for modern coccolithophores in tropical-subtropical regions, but
809 the lower temperature at high latitudes can approach the vital limits for coccolithophores (Baumann
810 et al., 1997), and become important as a bio-limiting factor.

811 Changes in the phytoplankton community could be related to a global influence of declining pCO_2.
812 Unfortunately the estimates from alkenone- and boron isotopes lack the resolution to unravel the
813 variation across and after the EOB (Fig. 5) in detail, and leave open the possibility that pCO_2 falling
814 below a certain threshold-level could have played a role in driving the reorganization in the
815 nannoplankton community. Alternatively, our combined biotic and geochemical proxy data (i.e.
816 nannofossil and benthic foraminiferal assemblages, and $\Delta\delta^{13}C_{P\text{-}B}$) suggest an increase in nutrient
817 and food supply just after the EOB (Fig. 6), which would have favored opportunistic taxa over low-
818 nutrient selected, specialist species. Most large reticulofenestrids (except *R. hillae* and *R. circus*
819 group) never recovered to previous abundances, despite a return to more stratified conditions after
820 Step 2. It is unlikely that increased dissolution above 87 mcd (33 Ma) explains the loss of large,
821 heavily calcified taxa, but the decrease in size of coccoliths may have also have led to enhanced
822 remineralization of organic matter and less food supply to the benthic communities.

823 There appears to be a latitudinal gradient in the timing of nannofossil abundance decreases. The
824 total abundance decreases were first detected in the Southern Ocean (late Eocene; Persico and Villa,

2004), then at mid-latitude (after the EOB; this study), and finally at the equator (after Step 2, as inferred from a decrease in nannofossil species diversity at Tanzanian sites; Dunkley Jones et al., 2008). This observation may suggest a direct temperature effect on nannoplankton abundance since nannofossil floras reflect the pattern of cooling, which started and was most pronounced at high latitudes. On the other hand, high-latitude cooling may have impacted the global nutrient regimes and ocean circulation. Since regional dissolution bias may also have affected the comparison of absolute coccolith abundance, additional studies on well-preserved material will be necessary to confirm the timing and character of the response at different latitudes and in different ocean basins. Nevertheless, a meridional gradient in biotic response is expected, given the different environmental sensitivities and biogeographic ranges of different phytoplankton species (e.g. Wei and Wise, 1990; Monechi et al., 2000; Persico and Villa, 2004; Villa et al., 2008), and the diachroneity of the onset of cooling (Pearson et al., 2008).

6 Conclusions

High-resolution analyses of the calcareous nannofossil and foraminiferal assemblages refine the biostratigraphy at ODP Site 1263 (Walvis Ridge), and demonstrate distinct assemblage and abundance changes in marine biota across the Eocene-Oligocene transition. The biotic response of calcareous nannoplankton was very rapid (~47 kyr), following the EOB by ~120 kyr and pre-dating the climatic Step 2 event by 200 kyr.

The ecological success of smaller-sized coccolithophore species *versus* the drastic decrease of large reticulofenestrids, and the overall decrease of nannoplankton productivity after the EOB likely affected the benthic foraminiferal community (e.g. decrease in rectilinear species due to changes in nannoplankton floras), with increased seasonality driving the transient increased abundance of phytodetritus-using species. After Step 2 and in particular after 33.3 Ma, both nannoplankton and benthic records at Site 1263 were affected by intensified dissolution and corrosivity of bottom waters.

We conclude that the planktonic community reacted to fast-changing environmental conditions, possibly seasonally increased nutrient supply to the photic zone, global cooling or lowered CO_2-availability, and/or the crossing of a threshold-level in the longer-term climate and environmental changes suggested by available proxy data, such as the transient pCO_2 decline during the late Eocene-early Oligocene.

Supplement data file contains: Table S1 (planktonic foraminiferal marker species); Tables S2 and S3 (loading species for datasets A and B); taxonomic remarks; Fig. S1 (plate of main species); Figs. S2 and S3 (plotted curves of all the distinguished species in datasets A and B).

Acknowledgments

The authors are grateful to the International Ocean Discovery Program (IODP) core repository in Bremen for providing samples for this research. The ODP (now IODP) was sponsored by the US National Science Foundation and participating countries under management of the Joint Oceanographic Institutions (JOI), Inc. We are thankful to Tom Dunkley Jones, Giuliana Villa and an anonymous reviewer for their constructive suggestions. We also thank Paul Pearson for his helpful comments. The project was financially supported by the Swedish Research Council (VR grant 2011-4866 to J.H.), by MIUR-PRIN grant 2010X3PP8J 005 (to S.M.), and by Spanish Ministry of Science and Technology (FEDER funds) Project CGL2011-23077 (grant BES-2012-058945 to A.L.). E.T. acknowledges the Geological Society of America and the Leverhulme Foundation (UK) for research support. We are grateful to Davide Persico and Nicolàs Campione for discussions on the statistical approach, and to Helen Coxall for helpful suggestions on the oxygen isotope stratigraphy.

References

Adams, C. G., Butterlin, J., and Samanta, B. K.: Larger foraminifera and events at the Eocene-Oligocene boundary in the Indo–West Pacific region, in*:* Terminal Eocene Events, edited by: Pomerol, C. and Premoli Silva, I., Elsevier, Amsterdam, 237–252, 1986.

Adler, M., Hensen, C., Wenzhöfer, F., Pfeifer, K., and Schulz, H. D.: Modelling of calcite dissolution by oxic respiration in supralysoclinal deep-sea sediments, Mar. Geol., 177, 167–189, 2001.

Agnini, C., Fornaciari, E., Rio, D., Tateo, F., Backman, J., and Giusberti, L.: Responses of calcareous nannofossil assemblages, mineralogy and geochemistry to the environmental perturbations across the Paleocene/ Eocene boundary in the Venetian Pre-Alps, Mar. Micropaleontol., 63, 19–38, 2006.

Agnini, C., Fornaciari, E., Raffi, I., Catanzariti, R., Pälike, H., Backman, J., and Rio, D.: Biozonation and biochronology of Paleogene calcareous nannofossils from low and middle latitudes, Newsletters on Stratigraphy, 47, 131–181, 2014.

Aitchison, J.: The statistical analysis of compositional data. Chapman and Hall, London, 416 pp., 1986.

Anderson, L. D. and Delaney, L. M.: Middle Eocene to early Oligocene paleoceanography from the Agulhas Ridge, Southern Ocean (Ocean Drilling Program Leg 177, Site 1090), Paleoceanography, 20, PA1013, doi:10.1029/2004PA001043, 2005.

Andruleit, H., Stäger, S., Rogalla, U., and Čepek, P.: Living coccolithophores in the northern Arabian Sea: ecological tolerances and environmental control. Mar. Micropaleontol., 49, 157–181, 2003.

Aubry, M.-P.: Late Paleogene calcareous nannoplankton evolution; a tale of climatic deterioration, in: Eocene-Oligocene Climatic and Biotic Evolution, edited by: Prothero, D. R. and Berggren, W. A., Princeton University Press, 272–309, 1992.

Auer, G., Piller, W. E., and Harzhauser, M.: High-resolution calcareous nannoplankton palaeoecology as a proxy for small-scale environmental changes in the Early Miocene, Mar. Micropaleontol., 111, 53–65, 2014.

Backman, J.: Quantitative calcareous nannofossil biochronology of middle Eocene through early Oligocene sediment from DSDP Sites 522 and 523, Abhandlungen der Geologischen Bundesanstalt, Vienna, 39, 21–31, 1987.

Barker, P. F. and Thomas, E.: Origin, signature and palaeoclimatic influence of the Antarctic Circumpolar Current, Earth Science Reviews, 66, 143–162, 2004.

Baumann, K.-H., Andruleit, H., Schröder-Ritzrau, A., and Samtleben, C.: Spatial and temporal dynamics of coccolithophore communities during non-production phases in the Norwegian-Greenland Sea, in: Contributions to the Micropaleontology and Paleoceanography of the Northern North Atlantic, edited by: Hass, H. C. and Kaminski, M. A., Grzybowski Foundation Special Publication, 5, 227–243, 1997.

Beaufort, L., Probert, I., and Buchet, N.: Effects of acidification and primary production on coccolith weight: Implications for carbonate transfer from the surface to the deep ocean, Geochem. Geophy. Geosy., 8, 1–18, 2007.

Benson, R. H.: The origin of the psychrosphere as recorded in changes of deep-sea ostracode assemblages, Lethaia, 8, 69–83, 1975.

Benton, M. J.: The Red Queen and the Court Jester: species diversity and the role of biotic and abiotic factors through time, Science, 323, 728–732, 2009.

Berger, W. H.: Deep-sea carbonates: evidence for a coccolith lysocline, Deep-Sea Research and Oceanographic Abstracts, 20, 917–921, 1973.

922 Berggren, W. A. and Pearson, P. N.: A revised tropical to subtropical Paleogene planktonic
923 foraminifera zonation, J. Foramin. Res., 35, 279–298, 2005.
924 Berggren, W. A., Kent, D. V., Swisher, C. C., and Aubry, M.-P. A revised Cenozoic geochronology
925 and chronostratigraphy, in: Geochronology, time scales and global stratigraphic correlation, SEPM
926 Spec. Publ., 54, 129–212, 1995.
927 Blaj, T., Backman, J., and Raffi, I.: Late Eocene to Oligocene preservation history and
928 biochronology of calcareous nannofossils from paleo-equatorial Pacific Ocean sediments, Riv. Ital.
929 Paleontol. S., 115, 67–85, 2009.
930 Boeckel, B., Baumann, K.-H., Henrich, R., and Kinkel, H.: Coccolith distribution patterns in South
931 Atlantic and Southern Ocean surface sediments in relation to environmental gradients, Deep-Sea
932 Res. Pt. I, 53, 1073–1099, 2006.
933 Bohaty, S. M., Zachos, J. C., and Delaney, M. L.: Foraminiferal Mg/Ca evidence for Southern
934 Ocean cooling across the Eocene/Oligocene transition, Earth Planet. Sc. Lett., 317, 251–261, 2012.
935 Bollmann, J., Brabec, B., Cortes, M., and Geisen, M.: Determination of absolute coccolith
936 abundances in deep-sea sediments by spiking with microbeads and spraying (SMS method), Mar.
937 Micropaleontol., 38, 29–38, 1999.
938 Bolton, C. T. and Stoll, H.: Late Miocene threshold response of marine algae to carbon dioxide
939 limitation, Nature, 500, 558–562, 2013.
940 Bordiga, M., Beaufort, L., Cobianchi, M., Lupi, C., Mancin, N., Luciani, V., Pelosi, N., and
941 Sprovieri, M.: Calcareous plankton and geochemistry from the ODP site 1209B in the NW Pacific
942 Ocean (Shatsky Rise): new data to interpret calcite dissolution and paleoproductivity changes of the
943 last 450 ka, Palaeogeogr. Palaeocl., 371, 93–108, 2013.
944 Bordiga, M., Bartol, M., and Henderiks, J.: Absolute nannofossil abundance estimates: Quantifying
945 the pros and cons of different techniques, Revue de micropaléontologie,
946 http://dx.doi.org/10.1016/j.revmic.2015.05.002, 2015.
947 Boscolo-Galazzo, F., Thomas, E., and Giusberti, L.: Benthic foraminiferal response to the Middle
948 Eocene Climatic Optimum (MECO) in the South-Eastern Atlantic (ODP Site 1263), Palaeogeogr.
949 Palaeocl., 417, 432–444, 2015.
950 Bown, P. R. and Dunkley Jones, T.: New Paleogene calcareous nannofossil taxa from coastal
951 Tanzania: Tanzania Drilling Project Sites 11 to 14, J. Nannoplankton Res., 28, 17–34, 2006.
952 Bown, P. R. and Young, J. R.: Techniques, in: Calcareous Nannofossil Biostratigraphy, edited by:
953 Bown, P. R., Chapman and Hall, Cambridge, 16–28, 1998.
954 Bown, P. R., Lees, J. A., and Young, J. R.: Calcareous nannoplankton evolution and diversity
955 through time, in: Coccolithiphores, edited by: Thierstein, H., R. and Young J. R., Springer Berlin

Heidelberg, 481–508, 2004.
Bown, P. R., Dunkley Jones, T., Lees, J. A., Randell, R. D., Mizzi, J. A., Pearson, P. N., Coxall, H. K., Young, J.R., Nicholas, C. J., Karega, A., Singano, J., and Wade, B. S.:A Paleogene calcareous microfossil Konservat-Lagerstätte from the Kilwa Group of coastal Tanzania, Geol. Soc. Am. Bull., 120, 3–12, 2008
Bremer, M. L. and Lohmann, G. P.: Evidence for primary control of the distribution of certain Atlantic Ocean benthonic foraminifera by degree of carbonate saturation, Deep-Sea Res., 29, 987–998, 1982.
Buccianti, A. and Esposito, P.: Insights into Late Quaternary calcareous nannoplankton assemblages under the theory of statistical analysis for compositional data, Palaeogeogr. Palaeocli., 202, 209–277, 2004.
Cachao, M. and Moita, M. T.: *Coccolithus pelagicus*, a productivity proxy related to moderate fronts off Western Iberia, Mar. Micropaleontol., 39, 131–155, 2000.
Coccioni, R.: The genera *Hantkenina* and *Cribrohantkenina* (foraminifera) in the Massignano section (Ancona, Italy), in: The Eocene–Oligocene boundary in the Marche-Umbria basin (Italy), edited by: Premoli Silva, I., Coccioni, R., and Montanari, A., International Subcommission on the Paleogene Stratigraphy, Eocene Oligocene Meeting, Ancona, Spec. Publ., 2, 81–96, 1988.
Coxall, H. K. and Pearson, P. N.: Taxonomy, biostratigraphy, and phylogeny of the Hantkeninidae (*Clavigerinella*, *Hantkenina*, and *Cribrohantkenina*), in: Atlas of Eocene Planktonic Foraminifera, edited by: Pearson, P. N., Olsson, R. K., Huber, B. T., Hemleben, C., and Berggren, W. A., Cushman Foundation Special Publication, 41, 216–256, 2006.
Coxall, H. K. and Pearson, P. N.: The Eocene-Oligocene transition, in: Deep-time perspectives on climate change: marrying the signal from computer models and biological proxies, edited by: Williams, M., et al., Geological Society (London), Micropalaeontological Society, 351–387, 2007.
Coxall, H. K. and Wilson, P. A.: Early Oligocene glaciation and productivity in the eastern equatorial Pacific: insights into global carbon cycling, Paleoceanography, 26, doi:10.1029/2010PA002021, 2011.
Coxall, H. K., Wilson, P. A., Pälike, H., Lear, C. H., and Backman, J.: Rapid stepwise onset of Antarctic glaciation and deeper calcite compensation in the Pacific Ocean, Nature, 433, 53–57, 2005.
Daniels, C. J., Sheward, R. M., and Poulton, A. J.: Biogeochemical implications of comparative growth rates of *Emiliania huxleyi* and *Coccolithus* species, Biogeosciences, 11, 6915–6925, doi:10.5194/bg-11-6915-2014, 2014.

De Kaenel, E. and Villa, G.: Oligocene-Miocene calcareous nannofossil biostratigraphy and paleoecology from the Iberia abyssal plain, in: Proceedings ODP, Scientific Results, College Station, TX (Ocean Drilling Program), 149, 79–145, 1996.

De Villiers, S.: Foraminiferal shell-weight evidence for sedimentary calcite dissolution above the lysocline. Deep-Sea Res. Pt. I, 52, 671-680, 2005.

DeConto, R. M. and Pollard, D.: Rapid Cenozoic glaciation of Antarctica induced by declining atmospheric CO_2, Nature, 421, 245–249, 2003.

Diester-Haass, L.: Middle Eocene to early Oligocene paleoceanography of the Antarctic Ocean (Maud Rise, ODP Leg 113, Site 689): change from low productivity to a high productivity ocean, Palaeogeogr. Palaeocl., 113, 311–334, 1995.

Diester-Haass, L. and Zachos, J. C.: The Eocene-Oligocene transition in the Equatorial Atlantic (ODP Site 325), paleoproductivity increase and positive $\delta^{13}C$ excursion, in: from greenhouse to icehouse: the marine Eocene-Oligocene transition, Prothero, D. R., Ivany, L. C., and Nesbitt, E. A., Columbia University Press, New York, 397–416, 2003.

Diester-Haass, L. and Zahn, R.: Eocene-Oligocene transition in the Southern Ocean: history of water mass circulation and biological productivity, Geology, 24, 163–166, 1996.

Dockery III, D. T.: Punctuated succession of marine mollusks in the northern Gulf Coastal Plain, Palaios, 1, 582–589, 1986.

Dunkley Jones, T., Bown, P. R., Pearson, P. N., Wade, B. S., Coxall, H. K., and Lear, C. H.: Major shift in calcareous phytoplankton assemblages through the Eocene-Oligocene transition of Tanzania and their implications for low-latitude primary production, Paleoceanography, 23, PA4204, doi:10.1029/2008PA001640, 2008.

Eldrett, J. S., Greenwood, D. R., Harding, I. C., and Hubber, M.: Increased seasonality through the Eocene to Oligocene transition in northern high latitudes, Nature, 459, 969–973, 2009.

Falkowski, P. G., Katz, M. E., Knoll, A. H., Quigg, A., Raven, J. A., Schofield, O., and Tayler, F. J. R.: The evolution of modern eukaryotic plankton, Science, 305, 354–360, 2004.

Fenero, R., Thomas, E., Alegret, L., and Molina, E.: Evolución paleoambiental del tránsito Eoceno-Oligoceno en el Atlántico sur (Sondeo 1263) basada en foraminíferos bentónicos, Geogaceta, 49, 3–6, 2010 (in Spanish).

Fioroni, C., Villa, G., Persico, D., and Jovane, L.: Middle Eocene-Lower Oligocene calcareous nannofossil biostratigraphy and paleoceanographic implications from Site 711 (equatorial Indian Ocean), Mar. Micropaleontol., 118, 50–62, 2015.

1021 Foster, L. C., Schmidt, D. N., Thomas, E., Arndt, S., and Ridgwell, A.: Surviving rapid climate
1022 change in the deep sea during the Paleogene hyperthermals, Proceedings of the National Academy
1023 of Sciences, 110, 9273–9276, 2013.
1024 Geisen, M., Bollmann, J., Herrle, J. O., Mutterlose, J., and Young, J. R.: Calibration of the random
1025 settling technique for calculation of absolute abundances of calcareous nannoplankton,
1026 Micropaleontology, 45, 437–442, 1999.
1027 Gibbs, S. J., Shackleton, N. J., and Young, J. R.: Identification of dissolution patterns in nannofossil
1028 assemblages: a high-resolution comparison of synchronous records from Ceara Rise, ODP Leg 154,
1029 Paleoceanography, 19, PA1029, doi:10.1029/2003PA000958, 2004.
1030 Gibbs, S. J., Young, J. R., Bralower, T. J., and Shackleton, N. J.: Nannofossil evolutionary events in
1031 the mid-Pliocene: an assessment of the degree of synchrony in the extinctions of *Reticulofenestra*
1032 *pseudoumbilicus* and *Sphenolithus abies*, Palaeogeogr. Palaeocl., 217, 155–172, 2005.
1033 Gibbs, S. J., Bown, P. R., Murphy, B. H., Sluijs, A., Edgar, K. M., Pälike, H., Bolton, C. T., and
1034 Zachos, J. C.: Interactive comment on "Scaled biotic disruption during early Eocene global
1035 warming events", Biogeosciences Discuss., 9, C618–C620, www.biogeosciences-
1036 discuss.net/9/C618/2012/, 2012.
1037 Giordano, M., Beardall, J., and Raven, A.: CO_2 concentrating mechanisms in algae: mechanisms,
1038 environmental modulation, and evolution, Annu. Rev. Plant. Biol., 56, 99–131, 2005.
1039 Goldner, A., Herold, N., and Huber, M.: Antarctic glaciation caused ocean circulation changes at
1040 the Eocene–Oligocene transition, Nature, 511, 574–578, 2014.
1041 Gooday, A. J.: Benthic foraminifera (Protista) as tools in deep-water palaeoceanography:
1042 environmental influences on faunal characteristics, Adv. Mar. Biol., 46, 1–90, 2003.
1043 Gooday, A. J. and Jorisssen, F. J.: Benthic foraminiferal biogeography: controls on global
1044 distribution patterns in deep-water settings, Annual Reviews of Marine Science, 4, 237–262, 2012.
1045 Gradstein, F. M., Ogg, J. G., Schmitz, M., and Ogg, G.: The Geologic Time Scale 2012, Vol. 2,
1046 Elsevier, 1144 pp., 2012.
1047 Griffith, E., Calhoun, M., Thomas, E., Averyt, K., Erhardt, A., Bralower, T., Lyle, M., Olivarez-
1048 Lyle, A., and Paytan, A.: Export productivity and carbonate accumulation in the Pacific Basin at the
1049 transition from greenhouse to icehouse climate (Late Eocene to Early Oligocene),
1050 Paleoceanography, 25: PA3212, doi:10.1029/2010PA001932, 2010.
1051 Hammer, Ø. and Harper, D. A. T.: Paleontological data analysis, Blackwell, Malden, USA, 2006.
1052 Hammer, Ø., Harper, D. A. T., and Ryan, P. D.: PAST: Paleontological Statistics Software Package
1053 for education and data analysis, Palaeontologia Electronica, 4, 1–9, http://palaeo-
1054 electronica.org/2001_2001/past/issue2001_2001.htm, 2001.

Hannisdal, B., Henderiks, J., and Liow, L. H.: Long-term evolutionary and ecological responses of calcifying phytoplankton to changes in atmospheric CO_2, Glob. Change Biol., 18, 3504–3516, 2012.

Haq, B. U. and Lohmann, G. P.: Early Cenozoic calcareous nannoplankton biogeography of the Atlantic Ocean, Mar. Micropaleontol., 1, 119–194, 1976.

Hayek, L.-A. C. and Buzas, M. A.: Surveying natural populations: quantitative tools for assessing biodiversity, Columbia University Press, 590 pp., 2010.

Hayward, B. W., Kawagata, S., Sabaa, A. T., Grenfell, H. R., van Kerckhoven, L., Johnson, K., and Thomas, E.: The last global extinction (Mid-Pleistocene) of deep-sea benthic foraminifera (Chrysalogoniidae, Ellipsoidinidae, Glandulonodosariidae, Plectofrondiculariidae, Pleurostomellidae, Stilostomellidae), their Late Cretaceous-Cenozoic history and taxonomy. Cushman Foundation For Foraminiferal Research, Spec. Publ., 43, 408 pp., 2012.

Henderiks, J.: Coccolithophore size rules - reconstructing ancient cell geometry and cellular calcite quota from fossil coccoliths, Mar. Micropaleontol., 67, 143–154, 2008.

Henderiks, J. and Pagani, M.: Refining ancient carbon dioxide estimates: significance of coccolithophore cell size for alkenone-based pCO_2 records, Paleoceanography, 22, PA3202, doi:10.1029/2006PA001399, 2007.

Henderiks, J. and Pagani, M.: Coccolithophore cell size and Paleogene decline in atmospheric CO_2, Earth Planet. Sc. Lett., 269, 576–584, 2008.

Henderiks, J., Winter, A., Elbrächter, M., Feistel, R., van der Plas, A. K., Nausch, G., and Barlow, R.: Environmental controls on *Emiliania huxleyi* morphotypes in the Benguela coastal upwelling system (SE Atlantic), Mar. Ecol. Prog. Ser., 448, 51–66, 2012.

Henson, S. A., Sanders, R., and Madsen, E.: Global patterns in efficiency of particulate organic carbon export and transfer to the deep ocean, Global Biogeochem. Cy., 26, GB1028, doi:10.1029/2011GB004099, 2012.

Hsü, K. J., LaBrecque, J. L., Carman Jr, M. F., and Shipboard Scientific Party: Site 522, in: DSDP, Initial Reports, College Station, TX, 73, 187–270, 1984.

Hyland, E., Murphy, B., Varela, P., Marks, K., Colwell, L., Tori, F., Monechi, S., Cleaveland, L., Brinkhuis, H., Van Mourik, C. A., Coccioni, R., Bice, D., and Montanari, A.: Integrated stratigraphic and astrochronologic calibration of the Eocene-Oligocene transition in the Monte Cagnero section (northeastern Apennines, Italy): a potential parastratotype for the Massignano global stratotype section and point (GSSP), in: The Late Eocene Earth: Hothouse, Icehouse, and Impacts, edited by: Koeberl, C. and Montanari, A., Geol. S. Am. S., 452, 303–322, 2009.

1088 Jennions, S. M., Thomas, E., Schimdt, D. N., Lunt, D., and Ridgwell, A.: Changes in benthic
1089 ecosystems and ocean circulation in the Southeast Atlantic across Eocene Thermal Maximum 2,
1090 Paleoceanography, 30, doi:10.1002/2015PA002821, 2015.
1091 Jorissen, F. J., de Stigter, H. C., and Widmark, J. G. V.: A conceptual model explaining benthic
1092 foraminiferal microhabitats, Mar. Micropaleontol., 26, 3–15, 1995.
1093 Jorissen, F. J., Fontanier, C., and Thomas, E.: Paleoceanographical proxies based on deep-sea
1094 benthic foraminiferal assemblage characteristics, in: Proxies in Late Cenozoic Paleoceanography:
1095 Pt. 2: Biological tracers and biomarkers, edited by: Hillaire-Marcel, C. and de Vernal, A., Elsevier,
1096 263–326, 2007.
1097 Katz, M. E., Miller, K. G., Wright, J. D., Wade, B. S., Browning, J. V., Cramer, B. S., and
1098 Rosenthal, Y.: Stepwise transition from the Eocene greenhouse to the Oligocene icehouse, Nat.
1099 Geosci., 1, 329–334, 2008.
1100 Keller, G: Stepwise mass extinctions and impact events: Late Eocene to early Oligocene, Mar.
1101 Micropaleontol., 10, 267–293, 1986.
1102 Kennett, J. P.: Cenozoic evolution of Antarctic glaciation, the circum-Antarctic Ocean, and their
1103 impact on global paleoceanography, J. Geophys. Res., 82, 3843–3860, 1977.
1104 Koch, C. and Young, J. R.: A simple weighing and dilution technique for determining absolute
1105 abundances of coccoliths from sediment samples, Journal of Nannoplankton Research, 29, 67–69,
1106 2007.
1107 Kucera, M. and Malmgren, B. A.: Logratio transformation of compositional data – a resolution of
1108 the constant sum constraint, Mar. Micropaleontol., 34, 117–120, 1998.
1109 Ladant, J.-B., Donnadieu, Y., and Dumas, C.: Links between CO_2, glaciation nd water flow:
1110 reconciling the Cenozoic history of the Antarctic Circumpolar Current, Clim. Past., 10, 1957-1966,
1111 2014.
1112 Lear, C. H., Bailey, T. R., Pearson, P. N., Coxall, H. K., and Rosenthal, Y.: Cooling and ice growth
1113 across the Eocene-Oligocene transition, Geology, 36, 251–254, 2008.
1114 Liu, Z., Tuo, S., Zhao, Q., Cheng, X., and Huang, W.: Deep-water earliest Oligocene Glacial
1115 Maximum (EOGM) in South Atlantic, Chinese Sci. Bull., 49, 2190–2197, 2004.
1116 Liu, Z., Pagani, M., Zinniker, D., DeConto, R. M., Huber, M., Brinkhuis, H., Shah, S. R., Leckie, R.
1117 M., and Pearson, A.: Global cooling during the Eocene-Oligocene climate transition, Science, 323,
1118 1187–1190, 2009.
1119 Lyle, M., Wilson, P. A., Janecek, T. R., et al.: Leg 199 Summary, in: Proceedings ODP, Initial
1120 Reports, College Station, TX (Ocean Drilling Program), 199, 1–87, 2002.
1121 MacArthur, R. H.: On the relative abundance of species, Am. Nat., 94, 25–36, 1960.

1122 Maiorano, P., Tarantino, F., Marino, M., and De Lange, G. J.: Paleoenvironmental conditions at
1123 Core KC01B (Ionina Sea) through MIS 13-9: evidence from calcareous nannofossil assemblages,
1124 Quatern. Int., 288, 97–111, 2013.
1125 Mancin, N., Hayward, B. H., Trattenero, I., Cobianchi, M., and Lupi, C.: Can the morphology of
1126 deep-sea benthic foraminifera reveal what caused their extinction during the mid-Pleistocene
1127 Climate Transition?, Mar. Micopaleontol., 104, 53–70, 2013.
1128 Marino, M. and Flores, J. A.: Middle Eocene to early Oligocene calcareous nannofossil stratigraphy
1129 at Leg 177 Site 1090, Mar. Micropaleontol., 45, 291–307, 2002.
1130 Maronna, R., Martin, R. D., and Yohai, V. J.: Robust statistics: Theory and methods, Wiley J., New
1131 York, 2006.
1132 Martini, E.: Standard Tertiary and Quaternary calcareous nannoplankton zonation, Proc. 2nd Conf.
1133 Planktonic Microfossils, Rome, 2, 739–786, 1971.
1134 Meng, J. and McKenna, M. C.: Faunal turnovers of Palaeogene mammals from the Mongolian
1135 Plateau, Nature, 394, 364–367, 1998.
1136 Merico, A., Tyrrell, T., and Wilson, P. A.: Eocene/Oligocene ocean de-acidification linked to
1137 Antarctic glaciation by sea-level fall, Nature 452, 979–982, 2008.
1138 Miller, K. G., Wright, J. D., Katz, M. E., Wade, B. S., Browning, J. V., Cramer, B. S., and
1139 Rosenthal, Y.: Climate threshold at the Eocene-Oligocene transition: Antarctic ice sheet influence
1140 on ocean circulation, Geol. Soc. Am. Spec. Pap., 452, 169–178, 2009.
1141 Milliman, J. D., Troy, P. J., Balch, W. M., Adams, A. K., Li, Y.-H., and Mackenzie, F. T.:
1142 Biologically mediated dissolution of calcium carbonate above the chemical lysocline? Deep-Sea
1143 Res. Pt. I, 46, 1653–1669, 1999.
1144 Mix, A. C., Morey, A. E., Pisias, N. G., and Hostetler, S. W.: Foraminiferal faunal estimates of
1145 paleotemperature: circumventing the no-analog problem yields cool ice age tropics,
1146 Paleoceanography, 14, 350–359, doi:10.1029/1999PA900012, 1999.
1147 Monechi, S., Buccianti, A., and Gardin, S.: Biotic signals from nannoflora across the iridium
1148 anomaly in the upper Eocene of the Massignano section: evidence from statistical analysis, Mar.
1149 Micropaleontol., 39, 219–237, 2000.
1150 Moolna, A. and Rickaby, R. E. M.: Interaction of the coccolithophore *Gephyrocapsa oceanica* with
1151 its carbon environment: response to a recreated high-CO_2 geological past, Geobiology, 10, 72–81,
1152 2012.
1153 Moore, T. C., Rabinowitz, P. D., et al.: Site 525-529, in: Deep Sea Drilling Project, Initial Reports,
1154 US Government Printing Office, Washington, DC, USA, 74, 41–465, 1984.
1155 Moore, T. C., Wade, B. S., Westerhold, T., Erhardt, A., M., Coxall, H. K., Baldauf, J., and Wagner,

M.: Equatorial Pacific productivity changes near the Eocene-Oligocene boundary, Paleoceanography, 29, 825–844, doi:10.1002/2014PA002656, 2014.
Norris, R. D., Wilson, P. A., Blum, P., and the Expedition 342 Scientists: Proceedings IODP, 342, College Station, TX (Integrated Ocean Drilling Program), doi:10.2204/iodp. proc.342.2014, 2014.
Ocean Drilling Stratigraphic Network, Plate Tectonic Reconstruction Service: http://www.odsn.de/odsn/services/paleomap/paleomap.html, last access: 10 April 2015, 2011.
Ortiz, S. and Thomas, E.: Deep-sea benthic foraminiferal turnover during the early middle Eocene transition at Walvis Ridge (SE Atlantic), Palaeogeogr. Palaeocl., 417, 126–136, 2015.
Pagani, M., Huber, M., Liu, Z., Bohaty, S. M., Henderiks, J., Sijp, W., Krishnan, S., and DeConto, R. M.: The role of carbon dioxide during the onset of Antarctic glaciation, Science, 334, 1261–1264, 2011.
Pälike, H., Norris, R. D., Herrle, J. O., Wilson, P. A., Coxall, H. K., Lear, C. H., Shackleton, N. J., Tripati, A. K., and Wade, B. S.: The heartbeat of the Oligocene climate system, Science, 314, 1894–1898, 2006.
Pea, L.: Eocene-Oligocene paleoceanography of the subantarctic South Atlantic: calcareous nannofossil reconstructions of temperature, nutrient, and dissolution history, Ph.D. thesis, Department of Earth Sciences, University of Parma, Italy, 210 pp., 2010.
Pearson, K.: Mathematical contributions to the theory of evolution. On a form of spurious correlation which may arise when indices are used in the measurement of organisms, P. R. Soc. London, 60, 489–498, 1896.
Pearson, P. N., van Dogen, B. E., Nicholas, C. J., Pancost, R. D., Schouten, S., Singano, J. M., and Wade, B. S.: Stable warm tropical climate through the Eocene Epoch, Geology, 35, 211–214, 2007.
Pearson, P. N., McMillan, I. K., Wade, B. S., Dunkley Jones, T., Coxall, H. K., Bown, P. R., and Lear, C. H.: Extinction and environmental change across the Eocene-Oligocene boundary in Tanzania, Geology, 36, 179–182, 2008.
Pearson, P. N., Gavin, L. F., and Wade, B. S.: Atmospheric carbon dioxide through the Eocene–Oligocene climate transition, Nature, 461, 1110–1114, 2009.
Peck, V. L., Yu, J., Kender, S., and Riesselman, C. R.: Shifting ocean carbonate chemistry during the Eocene-Oligocene climate transition: implications for deep-ocean Mg/Ca paleothermometry, Paleoceanography, 25, doi:10.1029/2009PA001906, 2010.
Persico, D. and Villa, G.: Eocene-Oligocene calcareous nannofossils from Maud Rise and Kerguelen Plateau (Antarctica): paleoecological and paleoceanographic implications, Mar. Micropaleontol., 52, 153–179, 2004.

Peterson, L. C. and Prell, W. L.: Carbonate dissolution in recent sediments of the eastern equatorial Indian Ocean: preservation patterns and carbonate loss above the lysocline, Mar. Geol., 64, 259–290, 1985.

Plancq, J., Grossi, V., Henderiks, J., Simon, L., and Mattioli, E.: Alkenone producers during late Oligocene–early Miocene revisited, Paleoceanography, 27, PA1202, doi:10.1029/2011PA002164, 2012.

Premoli Silva, I. and Jenkins, D. G.: Decision on the Eocene-Oligocene boundary stratotype, Episodes, 16, 379–382, 1993.

Raffi, I., Backman, J., Fornaciari, E., Pälike, H., Rio, D., Lourens, L., and Hilgen, F.: A review of calcareous nannofossil astrobiochronology encompassing the past 25 million years, Quaternary Sci. Rev., 25, 3113–3137, 2006.

Riesselman, C. R., Dunbar, R. B., Mucciarone, D. A., and Kitasei, S. S.: High resolution stable isotope and carbonate variability during the early Oligocene climate transition: Walvis Ridge (ODP Site 1263), in: Antarctica: A Keystone in a Changing World-Online Proceedings of the 10th ISAES, edited by: Cooper, A. K., Raymond, C. R., and the 10th ISAES Editorial Team, US Geol. Surv., doi:10.3133/of2007-1047.srp095, 2007.

Rost, B., Riebesell, U., Burkhardt, S., and Sültemeyer, D.: Carbon acquisition of bloom-forming marine phytoplankton, Limnol. Oceanogr., 48, 55–67, 2003.

Rugenstein, M., Stocchi, P., von der Heijdt, A., Dijkstra, H., and Brinkhuis, H.: Emplacement of Antarctic ice sheet mass circumpolar ocean flow, Global Planet. Change, 118, 16–24, 2014.

Saavedra-Pellitero, M., Flores, J. A., Baumann, K.-H., and Sierro, F. J.: Coccolith distribution patterns in surface sediments of Equatorial and Southeastern Pacific Ocean, Geobios, 43, 131–149, 2010.

Salamy, K. A. and Zachos, J. C.: Latest Eocene-early Oligocene climate change and Southern Ocean fertility: inferences from sediment accumulation and stable isotope data, Palaeogeogr. Palaeocl., 145, 61–77, 1999.

Sarnthein, M. and Winn, K.: Reconstruction of low and middle latitude export productivity, 30,000 years BP to present: implication for global carbon reservoir, in: Climate-Ocean Interaction, edited by: Schlesinger, M. E., Kluwer Academic Publishers, 319–342, 1990.

Schumacher, S. and Lazarus, D.: Regional differences in pelagic productivity in the late Eocene to early Oligocene - a comparison of southern high latitudes and lower latitudes, Palaeogeogr. Palaeocl., 214, 243–263, 2004.

Sijp, W. P., von der Heydt, A. S., Dijkstra, H. A., Flögel, S., Douglas, P. J., and Bijl, P. K.: The role of ocean gateways on cooling climate on long time scales, Global Planet. Change, 119, 1–22, 2014.

Spencer-Cervato, C.: The Cenozoic deep sea microfossil record: explorations of the DSDP/ODP sample set using the Neptune Database, Palaeontol. Electron., 2, 2, 270 pp., 1999.
Thomas, E.: Late Cretaceous through Neogene deep-sea benthic foraminifers (Maud Rise, Weddell Sea, Antarctica), in: Proceedings ODP, Scientific Results, College Station, TX (Ocean Drilling Program), 113, 571–594, 1990.
Thomas, E.: Middle Eocene - late Oligocene bathyal benthic foraminifera (Weddell Sea): faunal changes and implications for ocean circulation, in: Late Eocene-Oligocene climatic and biotic evolution, edited by: Prothero, D. R., and Berggren, W. A., Princeton University Press, 245–271, 1992.
Thomas, E.: Cenozoic mass extinctions in the deep sea: what disturbs the largest habitat on Earth?, in: Large ecosystem perturbations: causes and consequences, edited by: Monechi, S., Coccioni, R., and Rampino, M., Geol. S. Am. S., 424, 1–23, 2007.
Thomas, E. and Gooday, A. J.: Cenozoic deep-sea benthic foraminifers: tracers for changes in oceanic productivity?, Geology, 24, 355–358, 1996.
Tori, F.: Variabilità climatica e ciclicità nell'intervallo Eocene Oligocene: dati dai nannofossili calcarei, Ph.D. thesis, Department of Earth Sciences, University of Florence, Italy, 222 pp., 2008 (in Italian).
Villa, G., Fioroni, C., Pea, L., Bohaty, S., and Persico, D.: Middle Eocene-late Oligocene climate variability: calcareous nannofossil response at Kerguelen Plateau, Site 748, Mar. Micropaleontol., 69, 173–192, 2008.
Villa, G., Fioroni, C., Persico, D., Roberts, A. P., and Florindo, F.: Middle Eocene to Late Oligocene Antarctic glaciation/deglaciation and Southern Ocean productivity, Paleoceanography, 29, 223–237, doi:10.1002/2013PA002518, 2014.
Wade, B. S. and Pälike, H.: Oligocene climate dynamics, Paleoceanography, 19, PA4019, doi:10.1029/2004PA001042, 2004.
Wade, B. S. and Pearson, P. N.: Planktonic foraminiferal turnover, diversity fluctuations and geochemical signals across the Eocene/Oligocene boundary in Tanzania, Mar. Micropaleontol., 68, 244–255, 2008.
Wei, W. and Wise, S. W.: Biogeographic gradients of middle Eocene–Oligocene calcareous nannoplankton in the South Atlantic Ocean, Palaeogeogr. Palaeocl., 79, 29–61, 1990.
Winter, A., Jordan, R. W., and Roth, P. H.: Biogeography of living coccolithophores in ocean waters, in: Coccolithophores, edited by: Winter, A. and Siesser, W. G., 161–177, 1994.

1255 Young, J. R., Geisen, M., and Probert, I.: A review of selected aspects of coccolithophore biology
1256 with implications for paleodiversity estimation, Micropaleontology, 51,267–288,
1257 doi:10.2113/gsmicropal.51.4.267, 2005
1258 Young, J. R., Bown P.R., and Lees, J. A.: Nannotax3 website, International Nannoplankton
1259 Association, 21 Apr. 2014, URL: http://http://ina.tmsoc.org/Nannotax3, last access: 21 March 2015,
1260 2014.
1261 Zachos, J. C. and Kump, L. R.: Carbon cycle feedbacks and the initiation of Antarctic glaciation in
1262 the earliest Oligocene, Global Planet. Change, 47, 51–66, 2005.
1263 Zachos, J. C., Quinn, T. M., and Salamy, K. A.: High-resolution (104 years) deep-sea foraminiferal
1264 stable isotope records of the Eocene-Oligocene climate transition, Paleoceanography, 11, 251–266,
1265 doi:10.1029/96PA00571, 1996.
1266 Zachos, J., Pagani, M., Sloan, L., Thomas, E., and Billups, K.: Trends, rhythms, and aberrations in
1267 global climate 65 Ma to present, Science, 292, 686–693, 2001.
1268 Zachos, J. C., Kroon, D., Blum, P., and Shipboard Scientific Party: Site 1263, in: Proceedings ODP,
1269 Initial Reports, College Station, TX (Ocean Drilling Program), 208, 1–87, 2004.
1270 Zhang, J., Wang, P., Li, Q., Cheng, X., Jin, H., and Zhang, S.: Western equatorial Pacific
1271 productivity and carbonate dissolution over the last 550 kyr: foraminiferal and nannofossil evidence
1272 from ODP Hole 807A, Mar. Micropaleontol., 64, 121–140, 2007.
1273 Zhang, Y. G., Pagani, M., Liu, Z., Bohaty, S. M., and DeConto, R. M.: A 40-milion-year history of
1274 atmospheric CO_2, Philos. T. Roy. Soc. A., 371, 20130096, 2013.
1275

1276 **Table caption**

1277 **Table 1.** Calcareous nannofossil and planktonic foraminiferal (underlined) bioevents as identified in
1278 this study (at meter composite depth, mcd), and the mcd reported by the Shipboard Scientific Party
1279 (Zachos et al., 2004). Note that for the planktonic foraminiferal bioevents the average depth is
1280 reported. For each bioevent, the ages available in the most recent literature are given. N.A.: not
1281 available datum; *: ages not included in the sedimentation rate estimate.

1282

1283 **Figure captions**

1284 **Figure 1.** Paleogeographic reconstruction at 33 Ma (modified from Ocean Drilling Stratigraphic
1285 Network, Plate Tectonic Reconstruction Service,
1286 www.odsn.de/odsn/services/paleomap/paleomap.html) showing location of ODP Site 1263 (black

dot) on Walvis Ridge. The positions of the other sites (white squares) used for comparison and cited in the text are also given.

Figure 2. Eocene-Oligocene stratigraphy of Site 1263 and DSDP Site 522 (Walvis Ridge). Stable oxygen isotope stratigraphy ($\delta^{18}O$, ‰) DSDP Site 522 (Zachos et al., 1996) compared to that at Site 1263 (Riesselman et al., 2007). Absolute abundances of nannofossil marker species (N g^{-1}; note 10^7-10^8 change in scale among curves) for dataset A (grey line) and their relative percentages (%) for datasets A (black line) and B (black dashed). A 5 pt. smoothed curve is shown for the species *C. subdistichus*. Note the changes in horizontal scale among curves. Calcareous nannofossil and planktonic foraminiferal datums are highlighted. B: Base occurrence; T: Top occurrence; Bc: Base common occurrence.

Figure 3. Calcareous nannofossil abundance and distribution against depth (mcd) at Site 1263 (dataset A). $CaCO_3$ (wt%; Riesselman et al., 2007), coccolith dissolution index (%), H index, and the total absolute coccolith abundance (N g^{-1}). Error bars indicates the standard deviation (± 1 s.d., in %) of replicate counts. The absolute (N g^{-1}, black line) and relative (%, green line) abundances of the main species constituting the assemblage are shown. For *Cyclicargolithus* spp. and *C. pelagicus* the absolute abundances of different size groups are shown. The grey vertical bar marks an interval of major dissolution (87 to 83 mcd). The positions of EOB and Step 2 are reported.

Figure 4. Distribution patterns of PC1 **(a)** and PC2 **(b)** obtained from the PCA for the datasets A and B. Loadings of calcareous nannofossil taxa on the two principal components of the whole studied succession for dataset A are reported. The shaded boxes represent the most relevant loaded species. Shaded area: PCs (dataset A) obtained omitting the marker species in the dataset. Red line: PCs (dataset A) obtained inserting also the marker species. The positions of EOB and Step 2 are reported.

Figure 5. PC1 and cell-size trends during the Eocene-Oligocene at Site 1263. The average cell V:SA (μm) of all placolith-bearing species (green area), *Reticulofenestra-Dictyococcites-Cyclicargolithus* (red solid line) and *Reticulofenestra-Dictyococcites* (green dotted line) are reported. The average cell V:SA of ODP 925 (black circles; Pagani et al., 2011), DSDP 516 (white

1318 triangles; Henderiks and Pagani, 2008), DSDP 511-277 (white squares) and ODP 1090 (black
1319 squares) from the southern ocean (Pagani et al., 2011), and pCO_2 (ppm) alkenone-based from ODP
1320 925 (white circles; Pagani et al., 2011; Zhang et al., 2013), ODP 929 (black circles; Pagani et al.,
1321 2011), and pCO_2 boron isotope-based from TDP17/12 (grey triangles; Pearson et al., 2009) are also
1322 shown. For comparison with sea surface temperature (SST) proxies, the Mg/Ca (mmol/mol; Peck et
1323 al., 2010) at Site 1263 and the SST from $U^{k'}_{37}$ at low latitude in the Atlantic Ocean (Liu et al., 2009)
1324 are also displayed. The positions of EOB and Step 2 at Site 1263 are reported.

1325

1326 **Figure 6.** Paleoproductivity indices from nannofossil (PC2) and benthic foraminifer ($\Delta\delta^{13}C_{P\text{-}B}$
1327 calculated from data in Riesselman et al. (2007) and Peck et al. (2010); Fisher's alpha index -
1328 diversity proxy, extinction group species, phytodetritus-using species, buliminid species and the
1329 species *Nuttalides umbonifera*) datums are plotted against depth. The positions of EOB and Step 2
1330 are reported.

Table 1

	This study		Shipboard Scientific Party (Zachos et al., 2004)		Ages
Datum	**Interval (hole-core-section, cm)**	**Depth (mcd)**	**Average Depth (mcd)**	**Age (Ma)**	**References**
T *Isthmolithus recurvus*	B-3H-5, 115-116	83.19	86	32.7	Lyle et al. (2002)
T *Coccolithus formosus*	A-9H-4, 9-10	85.16	86	32.92	Pälike et al. (2006)
Bc *Sphenolithus akropodus*	A-9H-4, 100-102	86.34	N.A.		
B *Chiasmolithus altus*	B-4H-2, 131-132	89.4	N.A.	33.31*	Pälike et al. (2006)
B *Sphenolithus akropodus*	B-4H-3, 50-52	90.09	N.A.		
Bc *Clausicoccus subdistichus*	A-10H-4, 141-142	96.92	94.77	33.88*	Pälike et al. (2006)
T *Hantkenina* spp.	A-10H-5, 32-34/B-4H, CC	97.53	104.5	33.89	Gradstein et al. (2012)
Pseudohastigerina size reduction	A-10H-5, 32-34/B-4H, CC	97.53	N.A.	33.89	Gradstein et al. (2012)
T *Turborotalia cerroazulensis* group	A-10H-5, 32-34/B-4H, CC	97.53	N.A.		
T *Discoaster saipanensis*	B-5H-3, 50-52	102.27	104.1	34.44	Pälike et al. (2006)
T *Discoaster barbadiensis*	B-5H-4, 0-2	103.27	N.A.	34.77	Pälike et al. (2006)
B *Sphenolithus tribulosus*	B-5H-4, 50-52	103.77	N.A.		

Fig. 1

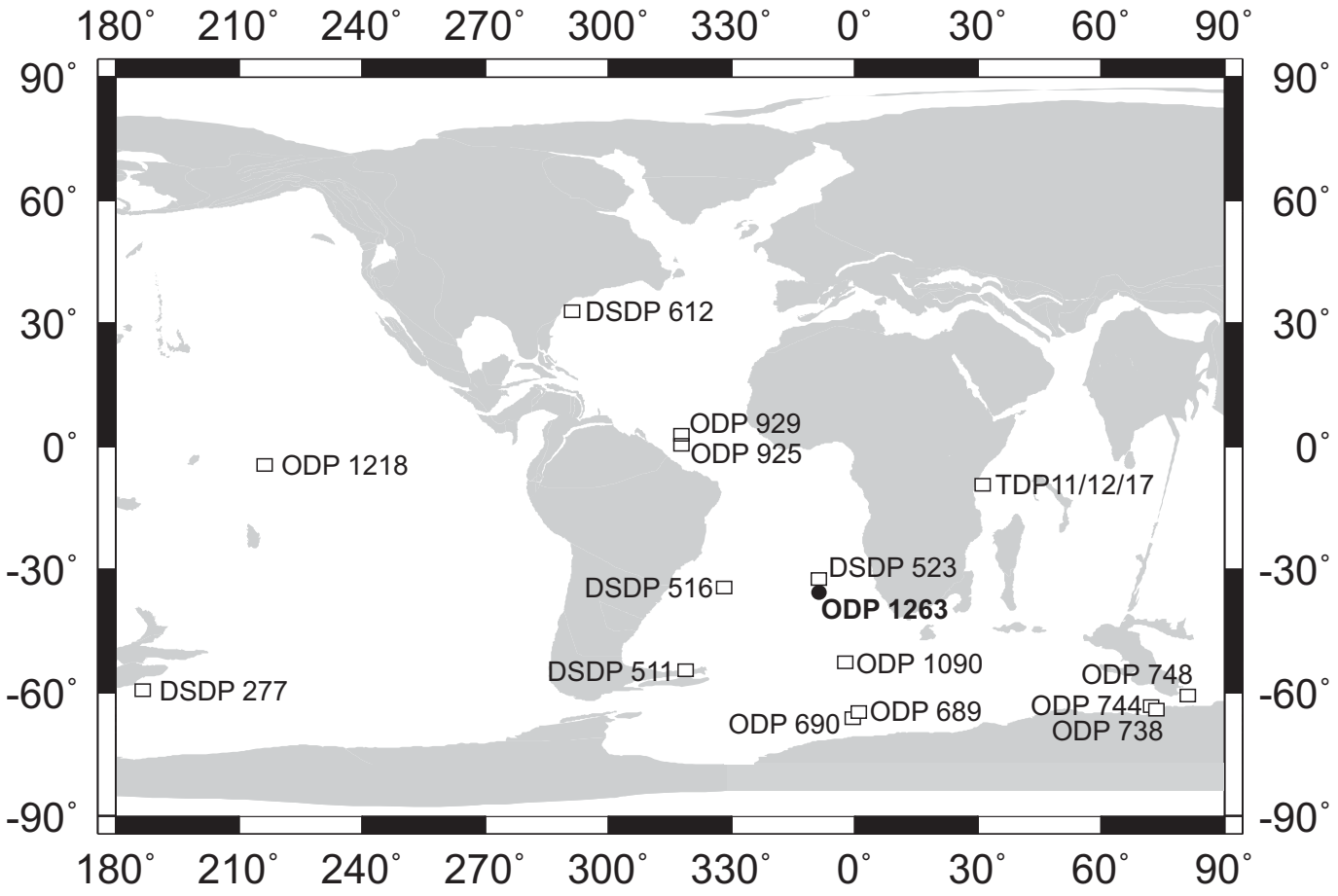
180˚ 210˚ 240˚ 270˚ 300˚ 330˚ 0˚ 30˚ 60˚ 90˚
90˚ 60˚ 30˚ 0˚ -30˚ -60˚ -90˚
DSDP 612
ODP 929
ODP 925
ODP 1218
TDP11/12/17
DSDP 523
DSDP 516
ODP 1263
DSDP 511
ODP 1090
ODP 748
DSDP 277
ODP 744
ODP 690
ODP 689
ODP 738

Fig. 2

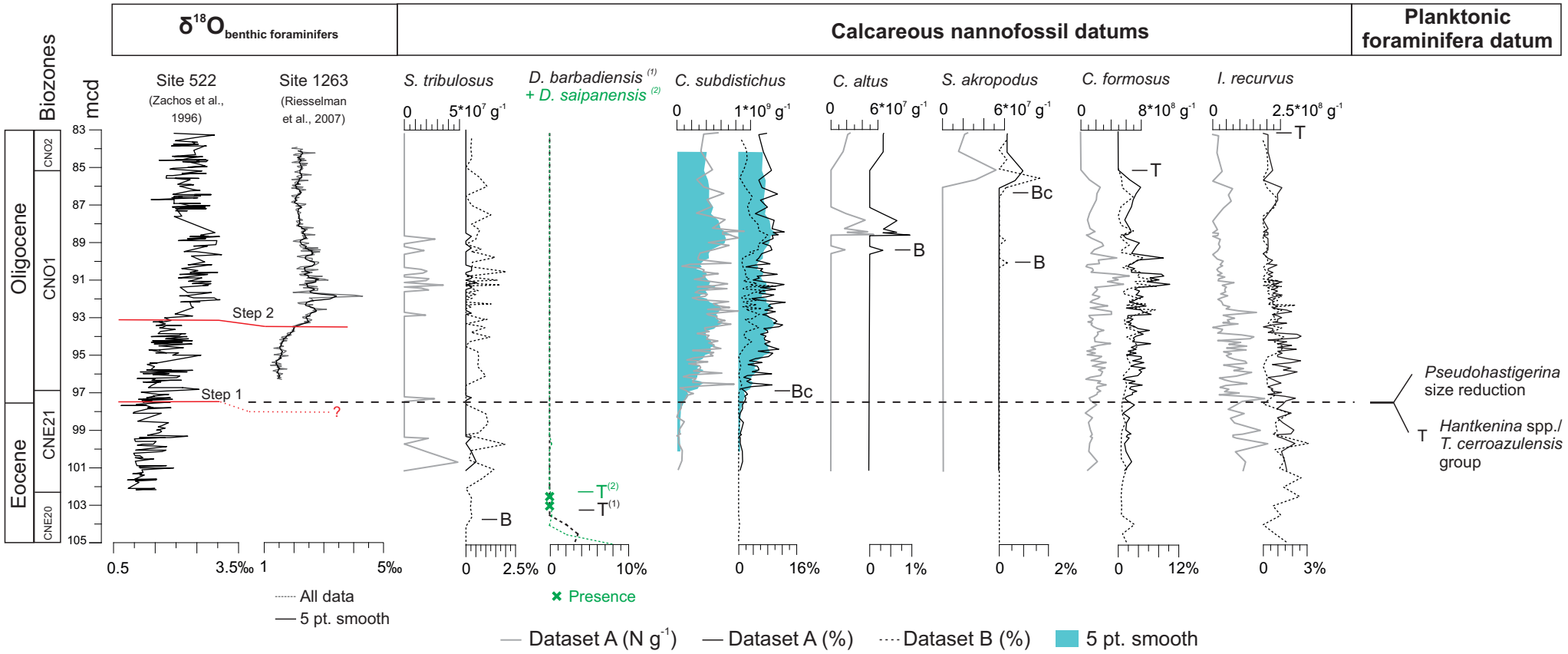
δ18O benthic foraminifers
Calcareous nannofossil datums
Planktonic foraminifera datum
Biozones
mcd
Oligocene
Eocene
CNO2
CNO1
CNE21
CNE20
Site 522
(Zachos et al., 1996)
Site 1263
(Riesselman et al., 2007)
Step 2
Step 1
?
S. tribulosus
D. barbadiensis (1)
+ D. saipanensis (2)
C. subdistichus
C. altus
S. akropodus
C. formosus
I. recurvus
B
T(2)
T(1)
Bc
T
Pseudohastigerina size reduction
Hantkenina spp./ T. cerroazulensis group
All data
5 pt. smooth
Presence
Dataset A (N g-1)
Dataset A (%)
Dataset B (%)
5 pt. smooth

Fig. 3

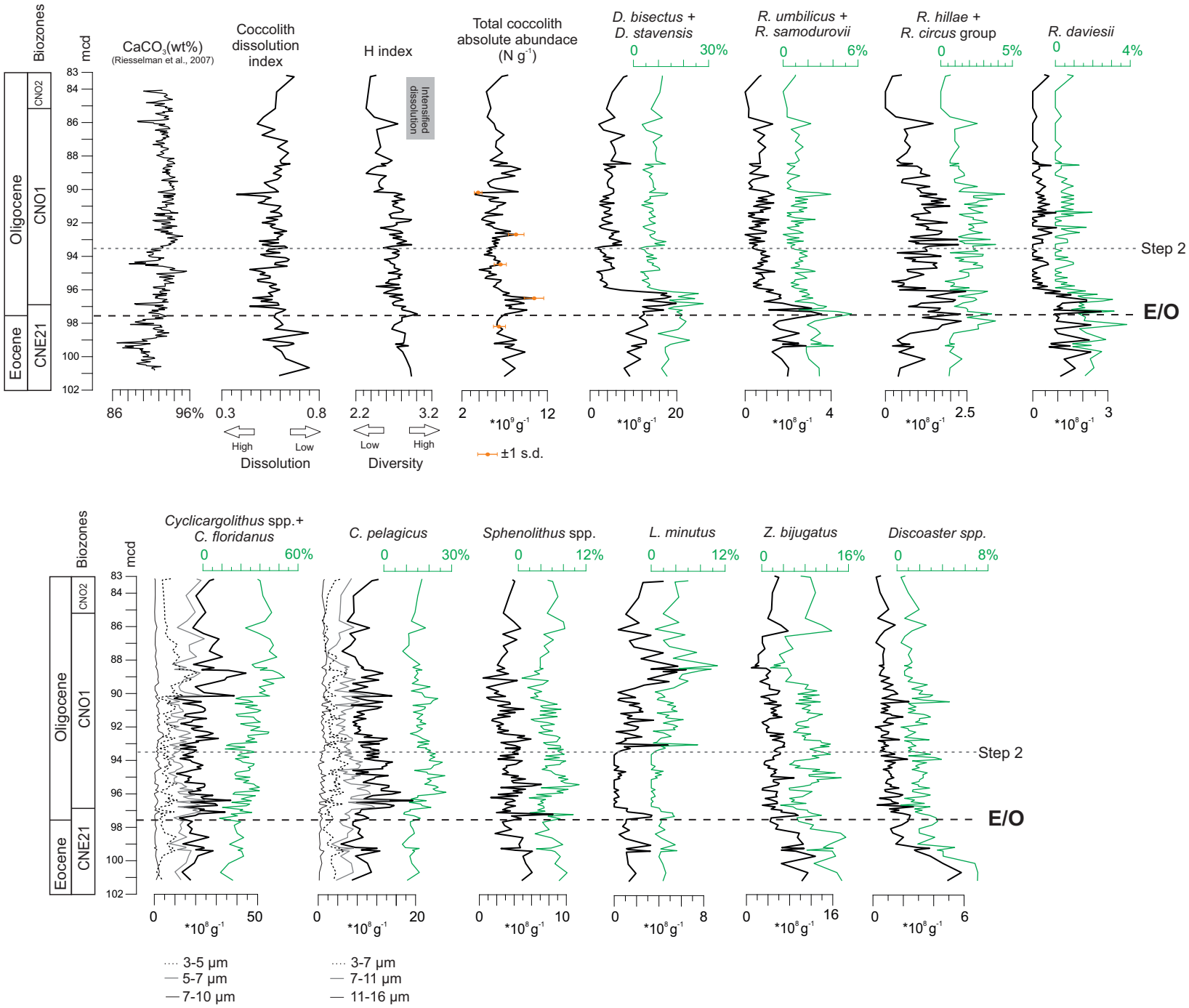
Biozones
mcd
Oligocene
Eocene
CNO2
CNO1
CNE21
CaCO3(wt%)
(Riesselman et al., 2007)
Coccolith dissolution index
H index
Intensified dissolution
Total coccolith absolute abundace (N g-1)
D. bisectus + D. stavensis
R. umbilicus + R. samodurovii
R. hillae + R. circus group
R. daviesii
Step 2
E/O
High
Low
Dissolution
Low
High
Diversity
±1 s.d.
Cyclicargolithus spp.+ C. floridanus
C. pelagicus
Sphenolithus spp.
L. minutus
Z. bijugatus
Discoaster spp.
3-5 µm
5-7 µm
7-10 µm
3-7 µm
7-11 µm
11-16 µm

Fig. 4

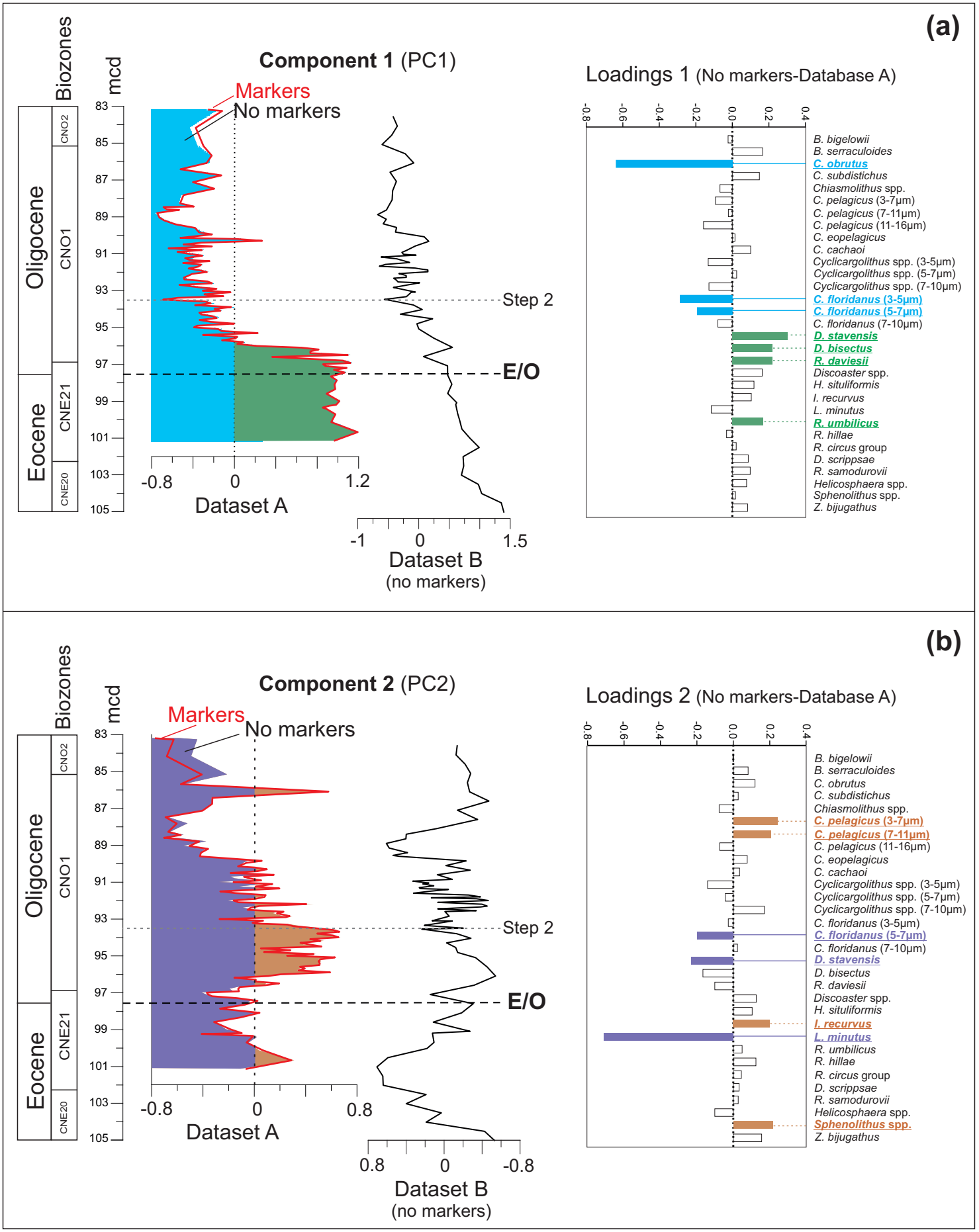
(a)
Biozones
Oligocene
Eocene
CNO2
CNO1
CNE21
CNE20
mcd
83
85
87
89
91
93
95
97
99
101
103
105
Component 1 (PC1)
Markers
No markers
Step 2
E/O
-0.8
0
1.2
Dataset A
-1
0
1.5
Dataset B
(no markers)
Loadings 1 (No markers-Database A)
-0.8
-0.6
-0.4
-0.2
0.0
0.2
0.4
B. bigelowii
B. serraculoides
C. obrutus
C. subdistichus
Chiasmolithus spp.
C. pelagicus (3-7µm)
C. pelagicus (7-11µm)
C. pelagicus (11-16µm)
C. eopelagicus
C. cachaoi
Cyclicargolithus spp. (3-5µm)
Cyclicargolithus spp. (5-7µm)
Cyclicargolithus spp. (7-10µm)
C. floridanus (3-5µm)
C. floridanus (5-7µm)
C. floridanus (7-10µm)
D. stavensis
D. bisectus
R. daviesii
Discoaster spp.
H. situliformis
I. recurvus
L. minutus
R. umbilicus
R. hillae
R. circus group
D. scrippsae
R. samodurovii
Helicosphaera spp.
Sphenolithus spp.
Z. bijugathus
(b)
Biozones
Oligocene
Eocene
CNO2
CNO1
CNE21
CNE20
mcd
83
85
87
89
91
93
95
97
99
101
103
105
Component 2 (PC2)
Markers
No markers
Step 2
E/O
-0.8
0
0.8
Dataset A
0.8
0
-0.8
Dataset B
(no markers)
Loadings 2 (No markers-Database A)
-0.8
-0.6
-0.4
-0.2
0.0
0.2
0.4
B. bigelowii
B. serraculoides
C. obrutus
C. subdistichus
Chiasmolithus spp.
C. pelagicus (3-7µm)
C. pelagicus (7-11µm)
C. pelagicus (11-16µm)
C. eopelagicus
C. cachaoi
Cyclicargolithus spp. (3-5µm)
Cyclicargolithus spp. (5-7µm)
Cyclicargolithus spp. (7-10µm)
C. floridanus (3-5µm)
C. floridanus (5-7µm)
C. floridanus (7-10µm)
D. stavensis
D. bisectus
R. daviesii
Discoaster spp.
H. situliformis
I. recurvus
L. minutus
R. umbilicus
R. hillae
R. circus group
D. scrippsae
R. samodurovii
Helicosphaera spp.
Sphenolithus spp.
Z. bijugathus

Fig. 5

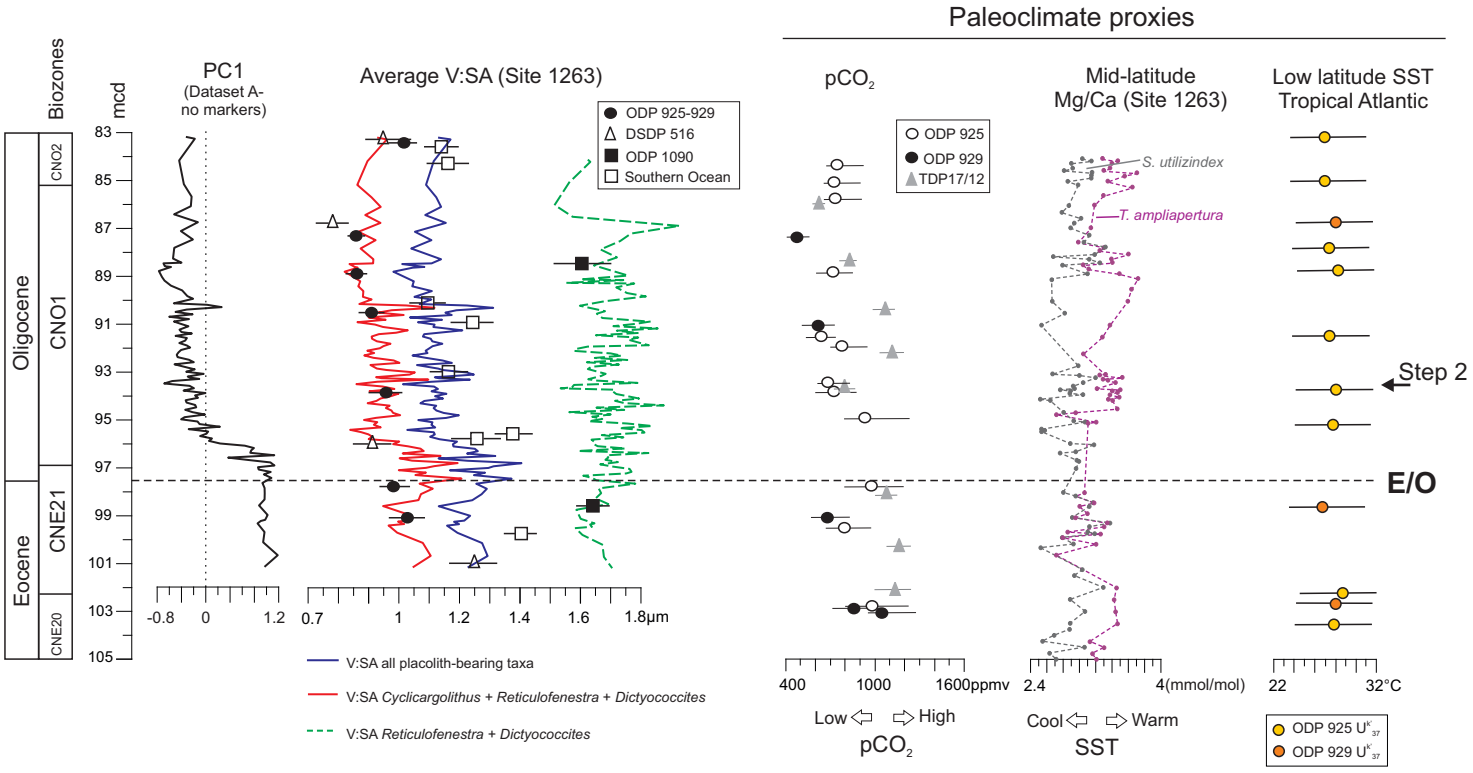
Paleoclimate proxies
Biozones
mcd
PC1
(Dataset A-
no markers)
Average V:SA (Site 1263)
ODP 925-929
DSDP 516
ODP 1090
Southern Ocean
pCO2
ODP 925
ODP 929
TDP17/12
Mid-latitude
Mg/Ca (Site 1263)
S. utilizindex
T. ampliapertura
Low latitude SST
Tropical Atlantic
Oligocene
Eocene
CNO2
CNO1
CNE21
CNE20
Step 2
E/O
-0.8
0
1.2
0.7
1
1.2
1.4
1.6
1.8µm
400
1000
1600ppmv
2.4
4(mmol/mol)
22
32°C
V:SA all placolith-bearing taxa
V:SA Cyclicargolithus + Reticulofenestra + Dictyococcites
V:SA Reticulofenestra + Dictyococcites
Low ⇦ ⇨ High
pCO2
Cool ⇦ ⇨ Warm
SST
ODP 925 U^K37
ODP 929 U^K37

Fig. 6

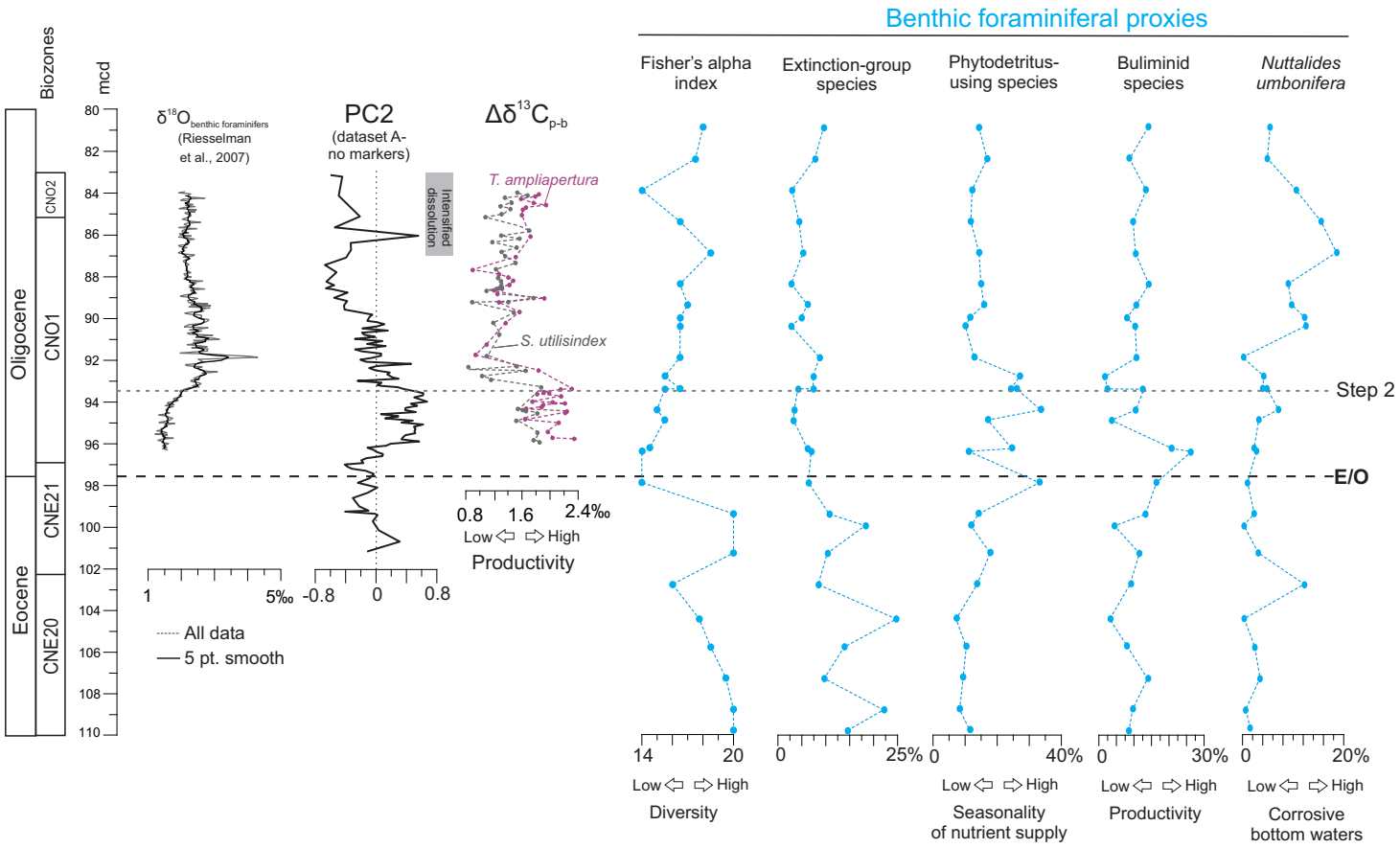
Benthic foraminiferal proxies
Biozones
mcd
Oligocene
Eocene
CNO2
CNO1
CNE21
CNE20
80
82
84
86
88
90
92
94
96
98
100
102
104
106
108
110
δ18O benthic foraminifers (Riesselman et al., 2007)
1
5‰
All data
5 pt. smooth
PC2 (dataset A-no markers)
-0.8
0
0.8
Intensified dissolution
ΔδC13p-b
T. ampliapertura
S. utilisindex
0.8
1.6
2.4‰
Low ⇦ ⇨ High
Productivity
Fisher's alpha index
14
20
Low ⇦ ⇨ High
Diversity
Extinction-group species
0
25%
Phytodetritus-using species
0
40%
Low ⇦ ⇨ High
Seasonality of nutrient supply
Buliminid species
0
30%
Low ⇦ ⇨ High
Productivity
Nuttalides umbonifera
0
20%
Low ⇦ ⇨ High
Corrosive bottom waters
Step 2
E/O